

Stepwise and large-magnitude negative shift in $\delta^{13}\text{C}_{\text{carb}}$ preceded the main marine mass extinction of the Permian–Triassic crisis interval

Genming Luo^{a,b}, Yongbiao Wang^a, Hao Yang^a, Thomas J. Algeo^c, Lee R. Kump^d, Junhua Huang^b, Shucheng Xie^{a,*}

^a Key Laboratory of Biogeology and Environmental Geology of Ministry of Education, China University of Geosciences, Wuhan 430074, People's Republic of China

^b State Key Laboratory of Geological Processes and Mineral Resources, China University of Geosciences, Wuhan 430074, People's Republic of China

^c Department of Geology, University of Cincinnati, Cincinnati, OH 45221-0013, USA

^d Department of Geosciences and Earth System Science Center, The Pennsylvania State University, University Park, PA 16802, USA

ARTICLE INFO

Article history:

Received 6 August 2010

Received in revised form 26 October 2010

Accepted 27 October 2010

Available online 31 October 2010

Keywords:

High-resolution $\delta^{13}\text{C}_{\text{carb}}$

Mass extinction

Permian–Triassic crisis interval

Episodic volcanism

Microbialite

South China

ABSTRACT

Large perturbations to the global carbon cycle occurred during the Permian–Triassic boundary mass extinction, the largest extinction event of the Phanerozoic Eon (542 Ma to present). Controversy concerning the pattern and mechanism of variations in the marine carbonate carbon isotope record of the Permian–Triassic crisis interval (PTCI) and their relationship to the marine mass extinction has not been resolved to date. Herein, high-resolution carbonate carbon isotope profiles ($\delta^{13}\text{C}_{\text{carb}}$), accompanied by lithofacies, were generated for four sections with microbialite (Taiping, Zuodeng, Cili, and Chongyang) in South China to better constrain patterns and controls on $\delta^{13}\text{C}_{\text{carb}}$ variation in the PTCI and to test hypotheses about the temporal relationship between perturbations to the global carbon cycle and the marine mass extinction event. All four study sections exhibit a stepwise negative shift in $\delta^{13}\text{C}_{\text{carb}}$ during the Late Permian–Early Triassic, with the shift preceding the end-Permian crisis being larger ($>3\%$) than that following it (1–2%). The pre-crisis shifts in $\delta^{13}\text{C}_{\text{carb}}$ are widely correlatable and, hence, represent perturbations to the global carbon cycle. The comparatively smaller shifts following the crisis demonstrate that the marine mass extinction event itself had at most limited influence on the global carbon cycle, and that both Late Permian $\delta^{13}\text{C}_{\text{carb}}$ shifts and the mass extinction must be attributed to some other cause. Their origin cannot be uniquely determined from C-isotopic data alone but appears to be most compatible with a mechanism based on episodic volcanism in combination with collapse of terrestrial ecosystems and soil erosion.

© 2010 Elsevier B.V. All rights reserved.

1. Introduction

The end-Permian mass extinction was the most severe biotic crisis of the Phanerozoic, during which more than 90% of species in the ocean and about 70% of vertebrate families on land were eliminated (Erwin, 1993; Erwin et al., 2002; Raup and Sepkoski, 1982; Sepkoski, 1989). Harsh environmental conditions following the main mass extinction event at ~252 Ma resulted in diminished body size among many of the surviving organisms (He et al., 2007; Luo et al., 2006, 2008; Payne et al., 2004; Twitchett, 2007). As long as 5 Myr was required for full recovery of marine ecosystems (Bottjer et al., 2008). The causes of the end-Permian mass extinction remain a topic of ongoing debate. Proposed mechanisms include massive volcanism (Kamo et al., 2003; Korte et al., 2010; Reichow et al., 2009; Renne et al., 1995), ocean anoxia (Algeo et al., 2007a; Grice et al., 2005; Isozaki, 1997; Kump et al., 2005; Meyer et al., 2008; Wignall and Twitchett,

1996), hypercapnia (Knoll et al., 1996, 2007), and bolide impact (Basu et al., 2003; Becker et al., 2004).

It has long been recognized that the end-Permian mass extinction was accompanied by a distinct perturbation in the global carbon cycle evidenced by large negative shifts in the carbon isotopic composition of both carbonates and organic matter (see Korte and Kozur, 2010, for a review). However, the temporal relationship of the mass extinction event to perturbations of the global carbon cycle is still controversial. One idea (Hypothesis A) is that the marine mass extinction occurred concurrently with a major perturbation to the carbon cycle (Krull et al., 2004; Twitchett et al., 2001; Wang et al., 2007) (Fig. 1). A second view is that the carbon cycle perturbation associated with the marine mass extinction significantly preceded the mass extinction event itself (Cao et al., 2002; Gorjan et al., 2008; Holser et al., 1989; Korte and Kozur, 2010; Luo et al., submitted for publication; Richoz et al., 2010; Xie et al., 2007). This model has two variants, one invoking a relatively small negative excursion ($<2\%$) leading up to the mass extinction event (Hypothesis B), and the other invoking a much larger negative excursion ($>2\%$) preceding the extinction (Hypothesis C; Fig. 1). As relatively little attention has been paid to date to the details of $\delta^{13}\text{C}_{\text{carb}}$ variation before the marine mass

* Corresponding author.

E-mail address: xiecutg@163.com (S. Xie).

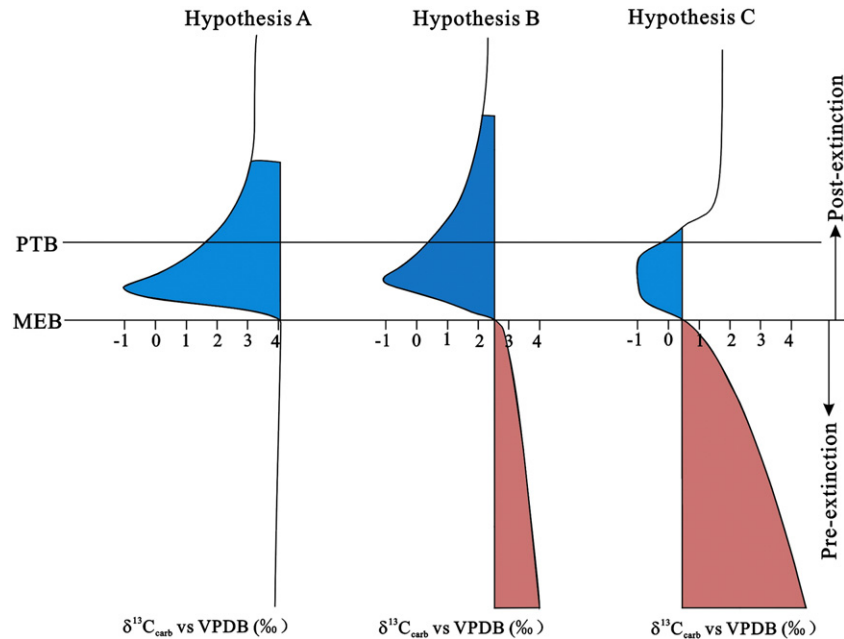


Fig. 1. Three proposed hypotheses for the temporal relationship between the main marine mass extinction and variations in $\delta^{13}\text{C}_{\text{carb}}$ in the PTCI. MEB = mass extinction boundary, PTB = Permian–Triassic boundary.

extinction, it is not clear whether Hypothesis B or Hypothesis C is more applicable to the Permian–Triassic Crisis Interval (PTCI).

Several recent studies have examined the timing and significance of shifts in Late Permian marine $\delta^{13}\text{C}_{\text{carb}}$ records. Korte and Kozur (2010) examined high-resolution Permian–Triassic (P–Tr) boundary sections in Iran and Europe, concluding that the negative shift in $\delta^{13}\text{C}_{\text{carb}}$ started within the *Clarkina bachmanni* conodont zone of the Late Permian Changhsingian Stage, about 0.45–0.50 Myr before the end-Permian crisis. Richoz et al. (2010) examined $\delta^{13}\text{C}_{\text{carb}}$ variation in several P–Tr boundary sections in the Neo-Tethyan region, showing that the magnitude of the negative shift in $\delta^{13}\text{C}_{\text{carb}}$ that preceded the end-Permian mass extinction was larger than that following it. They inferred that the negative shift started ~2.2 Myr before the P–Tr boundary, a much longer interval than that proposed by Korte and Kozur (2010). Neither of these studies devoted much attention to underlying processes and how they might be related to patterns of variation in the marine $\delta^{13}\text{C}_{\text{carb}}$ record. In this contribution, we report the results of C-isotopic analysis of four P–Tr boundary sections from South China containing microbialite units (Taiping, Zuodeng, Cili, and Chongyang). The aims of this paper are (1) to present high-resolution $\delta^{13}\text{C}_{\text{carb}}$ profiles for the study sections, (2) to analyze the pattern and timing of negative shifts in $\delta^{13}\text{C}_{\text{carb}}$ during the Late Permian–Early Triassic interval, (3) to test multiple hypotheses regarding the temporal relationship between Late Permian perturbations to the global carbon cycle and the end-Permian mass extinction event, and (4) to discuss the implications of these findings with respect to the ultimate mechanism(s) of the P–Tr boundary crisis.

2. Geological setting

2.1. Palaeogeography

During the P–Tr transition, the South China craton was located near the equator in the eastern Palaeo-Tethys Ocean (Fig. 2A). The Nanpanjiang Basin was a deep-water basin along the southeastern margin of the South China craton within which numerous low-relief carbonate banks appeared during the Late Permian and evolved into high-relief platforms during the Early Triassic (Lehrmann et al., 2003, 2006). The Taiping and Zuodeng sections were located in the interiors

of the Pingguo and Debao platforms, respectively (Fig. 2B). To the north of the Nanpanjiang Basin was the Jiangnan carbonate platform, which formed a shallow, east–west-oriented saddle across the South China craton that connected with the Palaeo-Tethys Ocean to both the north and the south. The Chongyang and Cili sections were located in the northern part of the Jiangnan platform (Fig. 2B).

2.2. Lithostratigraphy

Three distinct lithological members can be recognized in each of the four study sections (Figs. 3–6). The lowermost member is of Late Changhsingian age and consists of cherty to non-cherty skeletal limestone containing diverse normal-marine fossils such as brachiopods, fusulinids, non-fusulinid foraminifera, gastropods, sponges, bivalves, echinoderms, algae, and rare rugose corals. This member is located in the upper part of the Heshan Formation in the Taiping and Zuodeng sections, and in the upper part of the Changxing Formation in the Chongyang and Cili sections. Three whitish-grey ash beds are present in this member in the Taiping section (Fig. 3).

The second member (in ascending stratigraphic sequence) is microbialite, which consists of both thrombolite and stromatolite (Yang et al., in press) and varies in thickness among the four study sections: ~4.5 m at Taiping, ~7.0 m at Zuodeng, and ~6.7 m at Chongyang and Cili. The microbialite is faunally poor but contains some microgastropods, ostracodes, and conodonts (Lehrmann et al., 2003; Wang et al., 2009). The microbialite facies generally overlies the Changhsingian skeletal limestone member along a sharp lithologic contact that is correlative with the end-Permian mass extinction horizon (Lehrmann, 1999). In the four sections studied here, the skeletal limestone–microbialite contact is planar and shows no evidence of erosion or dissolution, although it is coincident with a low-relief stylolite in the Zuodeng section. Most studies have inferred continuous deposition across this contact (e.g., Lehrmann et al., 2003), although evidence of chemical dissolution at the contact exists in some shallow carbonate sections (Liu et al., 2007; Payne et al., 2007). Based on field observations and petrographic study, Collin et al. (2009) inferred the presence of a hiatus between the microbialite facies and the underlying skeletal limestone in the region of the Great Bank of Guizhou in South China, which is outside the area of the present study. The microbialite

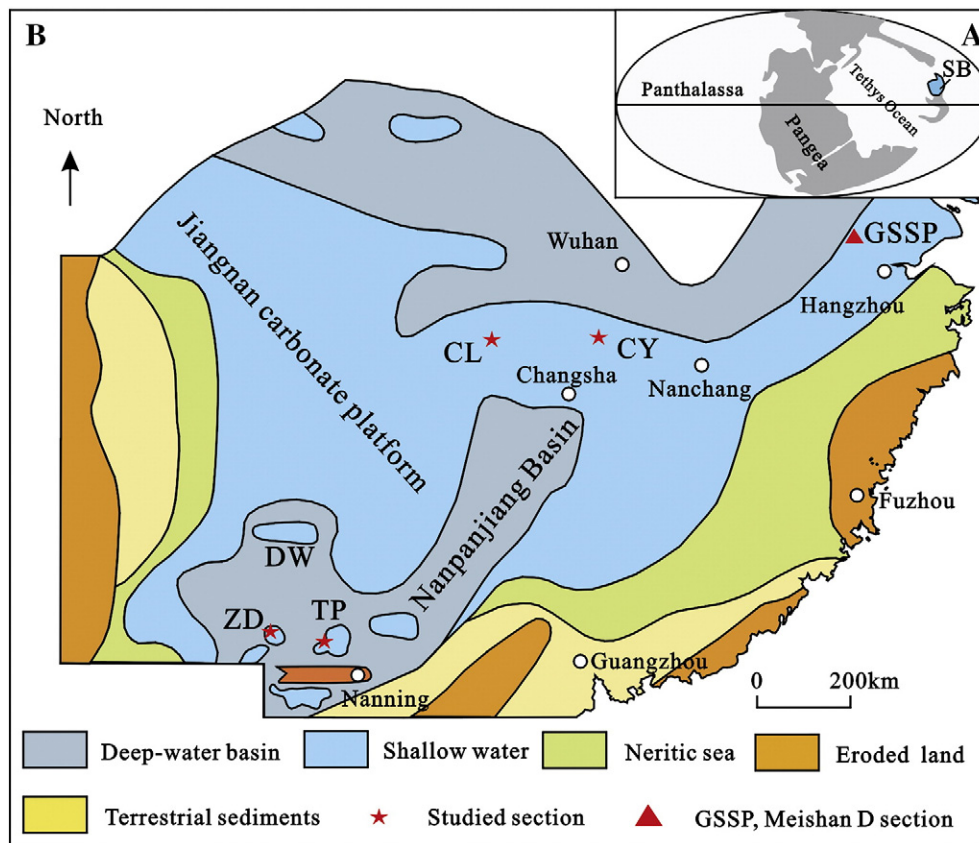


Fig. 2. A: Global paleogeographic reconstruction during the Permian–Triassic transition and location of the South China Block (modified from Corsetti et al., 2005). SB: South China Block. B: Paleogeography of the South China Block (Modified from Feng et al., 1997; Lehrmann et al., 2003) and sites distribution of the studied section. TP: the Taiping section; ZD: the Zuodeng section; CL: the Cili section; CY: the Chongyang section; GSSP: Global Stratotype Section and Point, the Meishan section.

represents a type of “disaster facies” that developed in shallow-water settings, particularly in South China (Wang et al., 2005) and other Tethyan locales (Baud et al., 2007; Pruss et al., 2006), immediately following the end-Permian mass extinction event.

The microbialite is overlain by the third member, which consists of thinly bedded limestone and oolitic limestone. The thinly bedded limestone is about 2–10 cm thick and structureless, with a few bivalves, such as *Claraia*, and gastropods. The oolitic limestone is thin and reddish in the Zuodeng section. A thin-bedded mudstone is located directly above the top of the microbialite layer in the Taiping and Zuodeng sections.

2.3. Biostratigraphy

The skeletal limestone is Late Changhsingian (latest Permian) in age. The upper Heshan Formation of the Taiping section contains typical uppermost Permian fusulinids including *Nankinella*, *Sphaerulina* and *Condofusulina*, as well as the conodont *Hindeodus latidentatus* (Wang et al., 1999). The upper Changxing Formation of the Cili section contains index fossils of the end-Permian *Palaeofusulina–Colaniella* zone (Wang et al., 2009). The P–Tr boundary, defined by the first appearance of the conodont *H. parvus*, is located in the microbialite layer somewhere above the base of the microbialite. *H. parvus* first appears ~1 m above the base of the microbialite in the Taiping section (Lehrmann et al., 2003; Yang et al., 1999) and 5.7 m and 3 m above the base of the microbialite in the Cili and Chongyang sections, respectively (Wang et al., 2009). The appearance of the conodont *H. latidentatus* in the lower part of the microbialite in the Taiping and Chongyang sections suggests that the deposition of the microbialite started in the latest Permian (Wang et al., 1999; Yang et al., 2006). This biostratigraphic framework is supported by a recent study of the

Dawen section from the Nanpanjiang Basin, which identified the conodont *H. parvus* ~7.5 m above the base of the microbialite (Chen et al., 2009). This study also reported the presence of *H. latidentatus*, *H. eurypyge* and *Clarkina zhejiangensis*, which are typical latest Permian elements (Jiang et al., 2007), in the lower part of the microbialite, suggesting the onset of the deposition of microbialite in the latest Permian. Although definitive zonal fossils have not been discovered to date in the Zuodeng section, we infer that it has a biostratigraphic framework similar to that of the nearby Taiping section.

3. Materials and methods

Large closely spaced fresh samples were collected from each of the main lithostratigraphic units in the four study sections. Previous studies have shown no distinct differences in $\delta^{13}\text{C}_{\text{carb}}$ between the spar and micrite of the thrombolite member of the microbialite (Luo et al., 2010; Mu et al., 2009), so we used bulk samples of microbialite for $\delta^{13}\text{C}_{\text{carb}}$ analysis in the present study. Weathered surfaces and large veins were trimmed off and each sample was cut into smaller pieces in the laboratory. Fresh chips were chosen and crushed to less than 100 mesh. The carbonate carbon isotope compositions were determined according to McCrea (1950). Under vacuum, the sample powder was reacted offline with 100% H_3PO_4 for 24 h at 25 °C. The carbon isotope composition of the generated CO_2 was measured on a Finnigan MAT 251 mass spectrometer. All isotopic data are reported as per mille (‰) relative to Vienna Pee Dee belemnite (V-PDB) standard. The analytical precision is better than $\pm 0.1\%$ for $\delta^{13}\text{C}$ and $\pm 0.2\%$ for $\delta^{18}\text{O}$ based on duplicate analyses.

We calculated several parameters from the $\delta^{13}\text{C}_{\text{carb}}$ profile of each study section. The magnitude of the pre-extinction shift in $\delta^{13}\text{C}_{\text{carb}}$ was defined as the difference between the average C-isotopic composition of

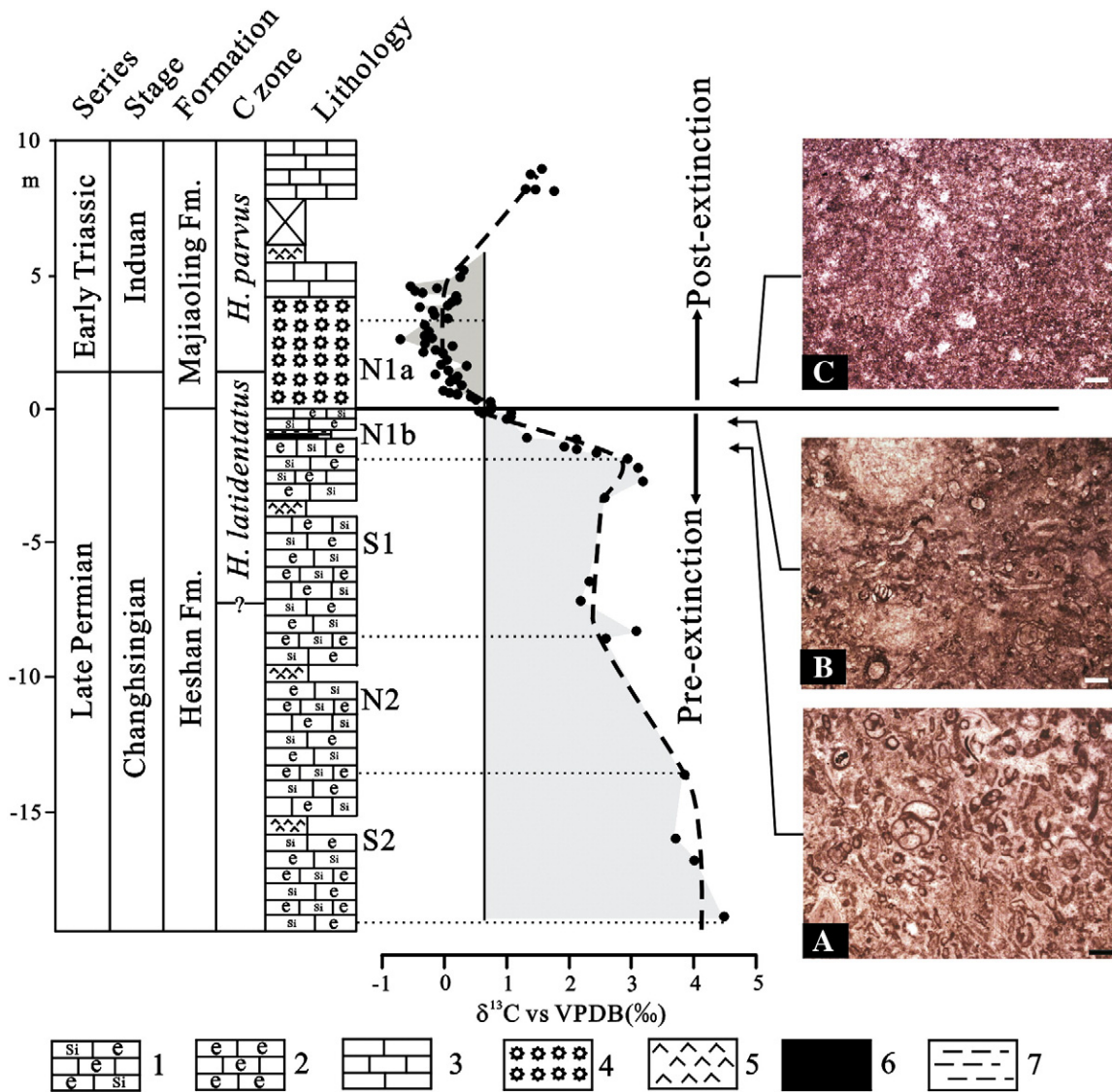


Fig. 3. Profile of the variation in $\delta^{13}\text{C}_{\text{carb}}$ during the P-Tr transition and thin sections from the underlying skeletal pack-limestone and the microbialite layer in the Taiping section. The coarse dashed line represents the variation trend in $\delta^{13}\text{C}_{\text{carb}}$. The arrows on the left side of the photos show stratigraphic level of the photos. Thin sections A and B are from the underlying skeletal limestone containing abundant fossils. A is located at 87 cm below the base of the microbialite. B is located at 33 cm below the base of the microbialite. Thin section C is from the base of the microbialite. C zone: conodont zone. 1: cherty skeletal limestone; 2: skeletal limestone; 3: thinly bedded limestone; 4: microbialite; 5: white clay bed; 6: chert bed; 7: mudstone. N: interval with gradual negative shift in $\delta^{13}\text{C}_{\text{carb}}$; S: interval with relatively stable in $\delta^{13}\text{C}_{\text{carb}}$; “b” and “a” indicate “below” and “above” the end-Permian mass extinction horizon, respectively. The scale bar is 0.1 mm.

a series of samples from the lower skeletal limestone yielding stable, relatively ^{13}C -enriched compositions and the $\delta^{13}\text{C}_{\text{carb}}$ of the uppermost sample of the skeletal limestone facies. The magnitude of the post-extinction shift in $\delta^{13}\text{C}_{\text{carb}}$ was defined as the difference in $\delta^{13}\text{C}_{\text{carb}}$ between the uppermost sample of the skeletal limestone and the most ^{13}C -depleted value in the overlying microbialite facies.

4. Results

4.1. Taiping section

At Taiping, $\delta^{13}\text{C}_{\text{carb}}$ ranges from +4.4‰ to -0.6‰, with the lowest values located in the microbialite layer (Fig. 3). The $\delta^{13}\text{C}_{\text{carb}}$ of the samples from the lower part of the skeletal limestone (S2) is about +4.0‰, a value that is typical of the Upper Permian in South China (Korte et al., 2005). $\delta^{13}\text{C}_{\text{carb}}$ starts to decline gradually ~13 m below the base of the microbialite (N2). The interval from 8 to 3 m below the base of the microbialite (S1) is characterized by relatively stable $\delta^{13}\text{C}_{\text{carb}}$ values. Prior to the first appearance of the microbialite, a

sharp and rapid negative shift in $\delta^{13}\text{C}_{\text{carb}}$ is present in the uppermost part of the skeletal limestone (N1b). The $\delta^{13}\text{C}_{\text{carb}}$ of the samples from top of the skeletal limestone is ~1‰ (Fig. 3). There is a gradual negative shift in $\delta^{13}\text{C}_{\text{carb}}$, from +0.7‰ to -0.5‰, in the lower part of the microbialite layer (N1a). In the upper part of the microbialite layer, the $\delta^{13}\text{C}_{\text{carb}}$ remains relatively stable around -0.5‰. In the lower part of the overlying thinly bedded limestone, the $\delta^{13}\text{C}_{\text{carb}}$ increases to +1.5 to +2‰ (Fig. 3).

4.2. Zuodeng section

At Zuodeng, the lower part of the skeletal limestone (S2) is characterized by $\delta^{13}\text{C}_{\text{carb}}$ values that fluctuate between +3 and +5‰ (Fig. 4). The overlying beds of the skeletal limestone are characterized by a gradual shift toward lower $\delta^{13}\text{C}_{\text{carb}}$ values, decreasing from +4.2‰ to less than +2‰ through a 5-m-thick interval (N2). Toward the top of the skeletal limestone, $\delta^{13}\text{C}_{\text{carb}}$ values stabilize at +1.8 to +2.5‰ within a 7-m-thick interval (S1) that extends almost to the base of the microbialite. The uppermost ~0.5 m of the skeletal

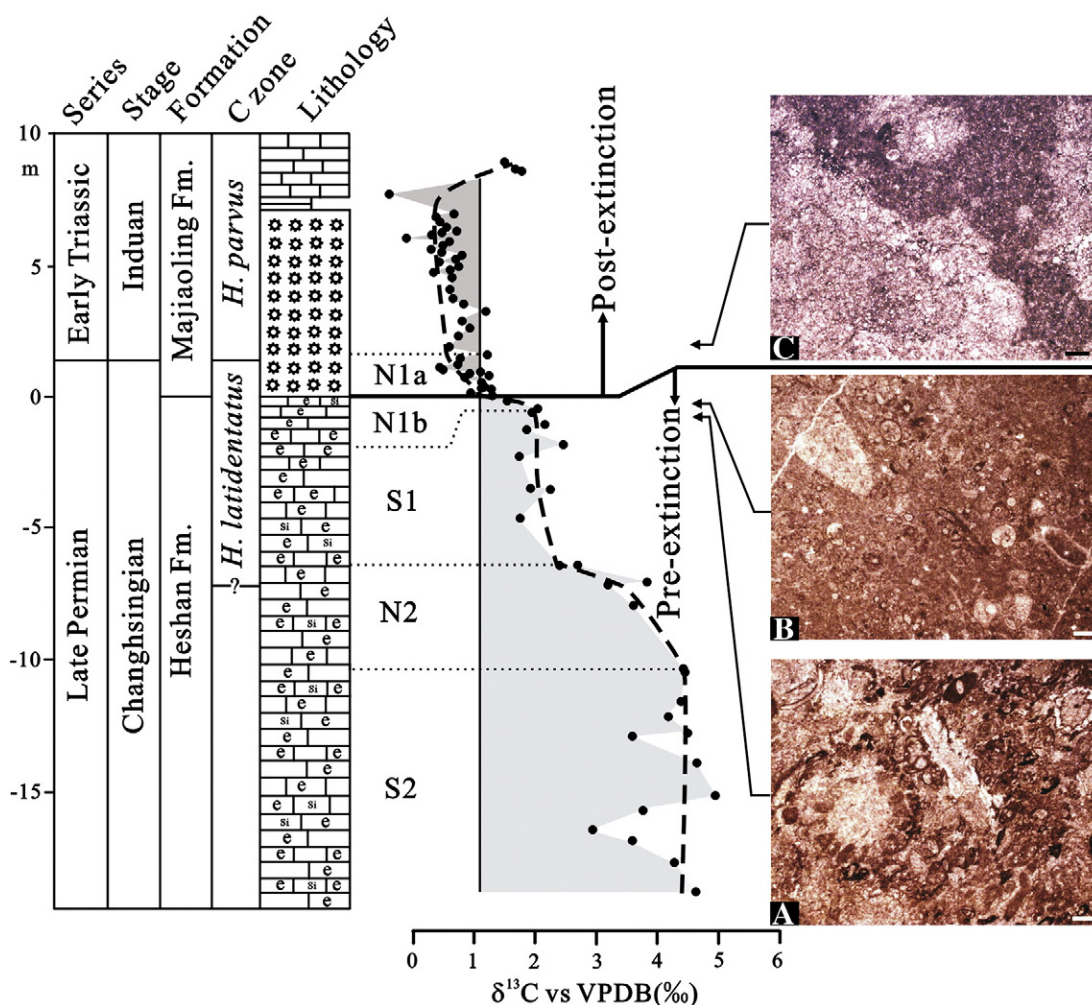


Fig. 4. Profile of the variation in $\delta^{13}\text{C}_{\text{carb}}$ in the PTCL and thin sections from the underlying skeletal limestone and the microbialite layer in the Zuodeng section. The coarse dashed line represents the variation trend in $\delta^{13}\text{C}_{\text{carb}}$. The arrows on the left side of the photos show stratigraphic level of the photos. Thin sections A and B are from the underlying skeletal limestone with abundant fossils, locating at 55 cm and 15 cm below the base of the microbialite, respectively. Thin section C is from the lower part of the microbialite layer. C zone: conodont zone. The lithology legend is the same as that in the Fig. 3. N: interval with gradual negative shift in $\delta^{13}\text{C}_{\text{carb}}$; S: interval with relatively stable in $\delta^{13}\text{C}_{\text{carb}}$; “b” and “a” indicate “below” and “above” the end-Permian mass extinction horizon, respectively. The scale bar is 0.1 mm.

limestone (N1b) exhibits a sharp negative shift in $\delta^{13}\text{C}_{\text{carb}}$, although of small amplitude ($\sim 1\%$). The $\delta^{13}\text{C}_{\text{carb}}$ of samples from the top of the skeletal limestone is about $+1.2\%$ (Fig. 4). In the first 20 cm above the skeletal limestone–microbialite contact, the $\delta^{13}\text{C}_{\text{carb}}$ profile shows a small (ca. -0.3%) negative shift followed by a small positive shift of similar magnitude. From this level, $\delta^{13}\text{C}_{\text{carb}}$ shifts rapidly from $+1.2\%$ to $+0.4\%$ through 50 cm of section and then gradually drops to $+0.1\%$ (with some fluctuations) through the next ~ 7 m (N1a; Fig. 4). A shift back toward relatively large $\delta^{13}\text{C}_{\text{carb}}$ values ($+2\%$) occurs in the lower part of the overlying thinly bedded limestone (Fig. 4).

4.3. Cili section

At Cili, $\delta^{13}\text{C}_{\text{carb}}$ values range from $+4.5\%$ to -0.8% (Fig. 5). The lower part of the skeletal limestone (S2) exhibits relatively stable $\delta^{13}\text{C}_{\text{carb}}$, around $+4.5\%$. In the overlying beds (N2), $\delta^{13}\text{C}_{\text{carb}}$ declines from $+4.5\%$ to $+2.5\%$ over a ~ 2 -m-thick interval. Toward the top of the skeletal limestone, from -10 m to -2 m (S1), $\delta^{13}\text{C}_{\text{carb}}$ values stabilize around $+2.5\%$. The uppermost 2 m of the skeletal limestone (N1b) is characterized by a sharp decline in $\delta^{13}\text{C}_{\text{carb}}$ to $+1.2\%$. The lower part of the microbialite shows a brief, small increase in $\delta^{13}\text{C}_{\text{carb}}$, followed by a gradual decline to values of 0 to -0.5% at 4 to 7 m (N1a; Fig. 5). A shift back toward heavier $\delta^{13}\text{C}_{\text{carb}}$ values is evident in the lower part of the overlying thinly bedded limestone.

4.4. Chongyang section

At Chongyang, $\delta^{13}\text{C}_{\text{carb}}$ values range from $+3\%$ to -0.4% (Fig. 6). The beds that are equivalent to the S2 and N2 intervals of the other three study sections are not exposed at this locale. The lowermost samples of the skeletal limestone (S1) yield $\delta^{13}\text{C}_{\text{carb}}$ values of $+3.0\%$. The upper 2 m of the skeletal limestone (N1b) exhibits a stepwise decline in $\delta^{13}\text{C}_{\text{carb}}$ from $+3.0\%$ to $+1.9\%$. In the lower 2.5 m of the microbialite layer, $\delta^{13}\text{C}_{\text{carb}}$ declines sharply from $+1.9\%$ to -0.4% (N1a) and then remains nearly stable through the overlying ~ 7 m of section (Fig. 6). In contrast to the sections discussed above, no shift back toward heavier $\delta^{13}\text{C}_{\text{carb}}$ values is evident in the 2 m of thin-bedded limestone sampled at the top of the Chongyang section.

5. Discussion

5.1. Evaluation of diagenetic overprinting

The carbon isotope composition of bulk samples with high carbonate content, such as the samples analyzed in this study, usually does not change significantly due to diagenesis because the carbon reservoir of the rock far exceeds the amount of carbon dissolved in diagenetic fluids (Marshall, 1992; Scholle and Arthur, 1980). Furthermore, several lines of evidence suggest that the primary carbon isotopic composition of the

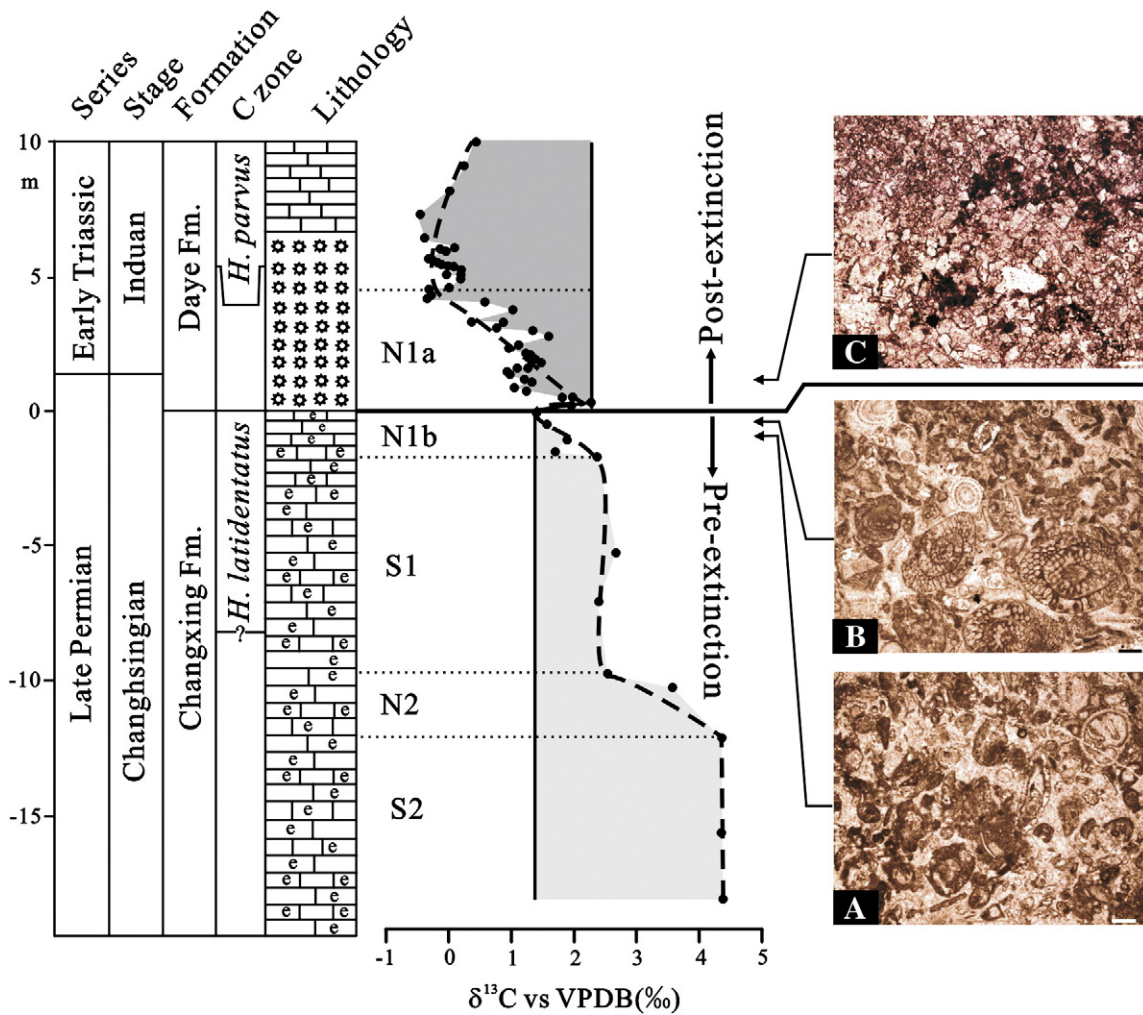


Fig. 5. Profile of the variation in $\delta^{13}\text{C}_{\text{carb}}$ in the PTCI and thin sections from the underlying skeletal limestone and the microbialite layer in the Cili section. The coarse dashed line represents the variation trend in $\delta^{13}\text{C}_{\text{carb}}$. The arrows on the left side of the photos show stratigraphic level of the photos. Thin sections A and B are from the underlying skeletal limestone with abundant fossils, locating at 45 cm and 4 cm below the base of the microbialite, respectively. Thin section C is from the lower part of the microbialite layer. C zone: conodont zone. The lithology legend is the same as that in the Fig. 3. N: interval with gradual negative shift in $\delta^{13}\text{C}_{\text{carb}}$; S: interval with relatively stable in $\delta^{13}\text{C}_{\text{carb}}$; "b" and "a" indicate "below" and "above" the end-Permian mass extinction horizon, respectively. The scale bar is 0.1 mm.

samples has been preserved to a large degree. First, the oxygen isotope compositions ($\delta^{18}\text{O}_{\text{carb}}$) of the samples are mostly -6% to -8% and, hence, not strongly depleted in ^{18}O as is typical of heavily diagenetically altered carbonates (Algeo et al., 1992). Second, no correlation exists between $\delta^{18}\text{O}_{\text{carb}}$ and $\delta^{13}\text{C}_{\text{carb}}$ overall (Fig. 7), in contrast with the positive correlation typical of diagenetically altered samples (Marshall, 1992). Third, Mn/Sr ratios in the Cili section (Luo et al., submitted for publication) and the other three study sections (Yongbiao Wang, unpublished data) are less than 2.0, far lower than the exclusion threshold of Kaufman and Knoll (1995), who inferred that primary $\delta^{13}\text{C}_{\text{carb}}$ signatures were retained when Mn/Sr < 10 . Fourth, secular variations in $\delta^{13}\text{C}_{\text{carb}}$ that track $\delta^{13}\text{C}$ variations in coeval P–Tr sections at other locations (see discussion later) also suggest that primary signatures have been preserved to a large degree.

Diagenesis has been a problem in some earlier C-isotopic studies of the PTCI, however. The problem is most severe in sections composed of calcareous mudstone or siltstone, in which carbonate concentrations are low and organic carbon concentrations sometimes high. In such sections, oxidation of organic matter (e.g., through sulphate reduction) can result in increased alkalinity in the diagenetic environment and precipitation of secondary carbonate phases that contain organic-derived, ^{13}C -depleted carbon (Irwin et al., 1977). Reports of $\delta^{13}\text{C}_{\text{carb}}$ minima (i.e., at the top of the N1a interval) of $< -5\%$ at Meishan (Nan and Liu, 2004; Xu and Yan, 1993) and

elsewhere (Haas et al., 2007; Twitchett et al., 2001) are entirely from such carbonate-poor lithologies. In contrast, carbonate-rich sections almost uniformly yield $\delta^{13}\text{C}_{\text{carb}}$ minima of -2% to 0% (Algeo et al., 2007a; Baud et al., 1989; Cao et al., 2002; Corsetti et al., 2005; Dolenc et al., 2001; Gorjan et al., 2008; Holser et al., 1989; Korte and Kozur, 2010; Korte et al., 2004; Krull et al., 2004; Payne et al., 2004; Xie et al., 2007), which is confirmed by C-isotopic profiles of the present study sections as well (Fig. 8). Recent restudy of the Meishan section has yielded C-isotopic records that are more free of diagenetic artifacts (Cao et al., 2002; Riccardi et al., 2007; Xie et al., 2007).

5.2. Timing and magnitude of the pre-extinction $\delta^{13}\text{C}_{\text{carb}}$ shifts during PTCI

In the Taiping, Zuodeng, and Cili sections, the $\delta^{13}\text{C}_{\text{carb}}$ of the lower part of the skeletal limestone (S2) is around $+4.0\%$ to 4.5% , values that are typical of the Upper Permian in South China (Korte et al., 2005) and that we regard as the marine carbonate baseline prior to the onset of Late Permian perturbations to the carbon cycle. From this baseline, the $\delta^{13}\text{C}_{\text{carb}}$ profiles of the four study sections show that a large negative shift occurred well before the end-Permian marine mass extinction horizon (Figs. 3–6). This shift is recorded as a pattern of two steps (N2 and N1b) in the three study sections (Cili, Taiping, and Zuodeng) that contain a greater thickness of Upper Permian

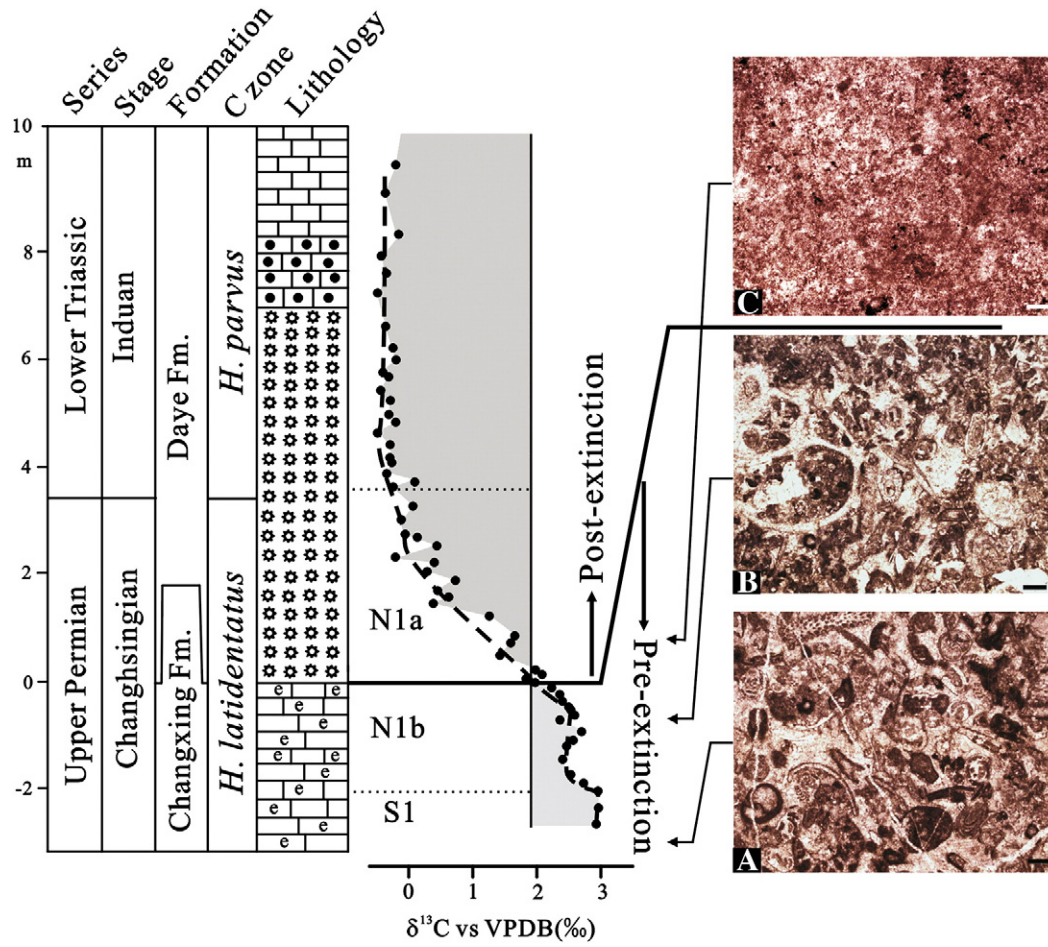


Fig. 6. Profile of the variation in $\delta^{13}\text{C}_{\text{carb}}$ in the PTCI and thin sections from the underlying skeletal limestone and the microbialite layer in the Chongyang section. The coarse dashed line represents the variation trend in $\delta^{13}\text{C}_{\text{carb}}$. The arrows on the left side of the photos show stratigraphic level of the photos. Thin sections A and B are from the underlying skeletal limestone with abundant fossils, locating at 203 cm and 83 cm below the base of the microbialite, respectively. Thin section C is from the microbialite layer. C zone: conodont zone. The lithology legend is the same as that in the Fig. 3. N: interval with gradual negative shift in $\delta^{13}\text{C}_{\text{carb}}$; S: interval with relatively stable in $\delta^{13}\text{C}_{\text{carb}}$; “b” and “a” indicate “below” and “above” the end-Permian mass extinction horizon, respectively. The scale bar is 0.1 mm.

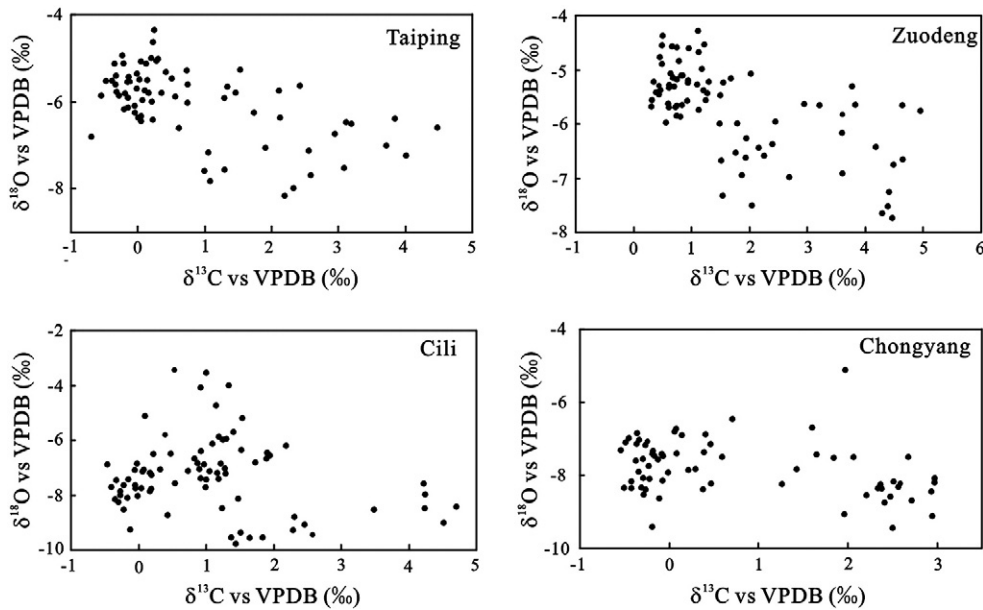


Fig. 7. Cross-plot between the carbon and oxygen isotopic composition of carbonate in the PTCI in the studied sections.

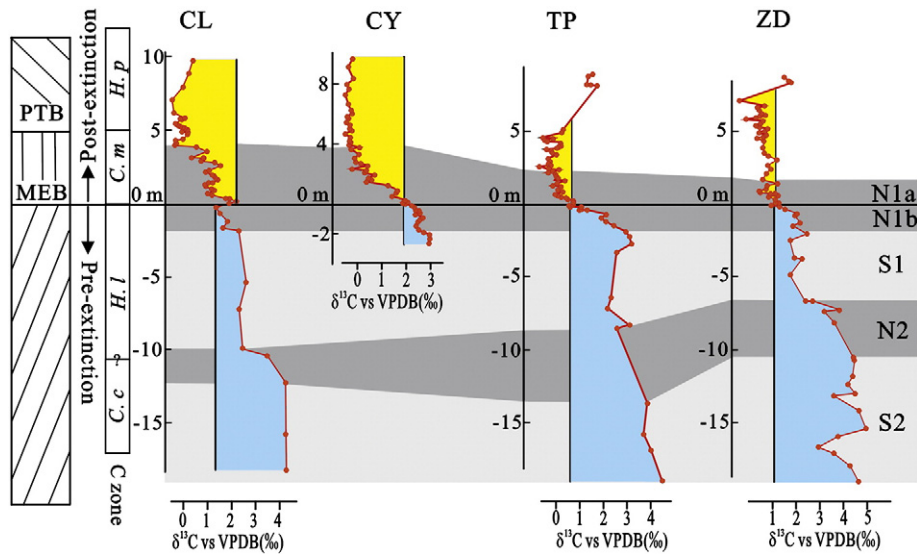


Fig. 8. Correlation of the $\delta^{13}\text{C}_{\text{carb}}$ profile in the PTCI in the four study sections in South China. See the Fig. 2 for locations of these sections. The conodont zones (C zone) were according to the paleontological data in the four sections and the correlation with the Meishan D section in South China. *H. p.*: *Hindeodus parvus* zone; *C. m.*: *Clarkina meishanensis* zone; *H. l.*: *H. latidentatus* zone; *C. c.*: *C. changhsingensis* zone. MEB: mass extinction boundary; PTB: Permian–Triassic boundary.

section, whereas only a single step (N1b) is recorded in the comparatively shorter Chongyang section (Fig. 8). The $\delta^{13}\text{C}_{\text{carb}}$ values of samples from the tops of the skeletal limestone in the four study sections (+1.2‰ to +1.9‰) are similar to those of other P–Tr boundary sections in South China, such as Meishan D (+1.3‰; Xie et al., 2007). Some sections in the Nanpanjiang Basin also have low $\delta^{13}\text{C}_{\text{carb}}$ in the uppermost skeletal limestone (Loufangwan: 0‰, Cui et al., 2008; Dawen: 0‰, Chen et al., 2009). Thus, our high-resolution C-isotopic records clearly invalidate Hypothesis A, which invokes no significant change in marine carbonate C-isotopic values prior to the end-Permian crisis (Fig. 1). Hypothesis A was previously advocated based on study of the Taiping section (Krull et al., 2004) as well as other sections (Wang et al., 2007), but both of these studies generated low-resolution datasets with limited biostratigraphic control.

The magnitude of the negative C-isotopic shift from the Upper Permian baseline to the top of the skeletal limestone is about 3.3‰ in all three of the thicker study sections (i.e., from +4.0‰ to +0.7‰ at Taiping, and from +4.5‰ to +1.2‰ at both Zuodeng and Cili; Fig. 8). The less complete Chongyang section shows a negative shift of only 1.1‰ (i.e., from +3.0‰ to +1.9‰). However, the C-isotopic composition of samples at the top of the skeletal limestone at Chongyang is similar to those of the more complete study sections, suggesting that the Chongyang section, if sampled fully, would yield a Late Permian C-isotopic shift of similar magnitude to the other study sections. The magnitude of these Late Permian C-isotopic shifts is significantly larger than 2.0‰ and, favoring Hypothesis C (i.e., a large pre-end-Permian shift) over Hypothesis B (i.e., a small pre-end-Permian shift). Other P–Tr boundary sections for which a sufficient stratigraphic interval of Upper Permian carbonates has been measured show negative C-isotopic shifts of comparable magnitude. For example, sections in the western Paleotethys and Neo-Tethys regions exhibit pre-end-Permian shifts that are mostly between 2.5‰ and 3.5‰ (Fig. 9; Dolenc et al., 2001; Korte and Kozur, 2005, 2010; Richoz et al., 2010).

The onset of the Late Permian C-isotopic shift has been stratigraphically constrained to the early or mid-Changhsingian Stage. In the Meishan section in South China, the negative shift starts in the lowermost part of bed 23 (Cao et al., 2002, 2009; Luo et al., 2010; Xie et al., 2007), about 40 m above the base of the Changhsingian and only 2 m below the end-Permian mass extinction horizon. The level is in the middle of the *Clarkina changhsingensis* Zone (below the *yini* Zone) and, thus, of mid-Changhsingian age. However, the onset of the C-isotopic shift may have occurred somewhat earlier in Upper

Permian sections in Iran and Europe. According to Richoz et al. (2010), the negative shift in $\delta^{13}\text{C}_{\text{carb}}$ began during deposition of the lower *Dzhulfites* beds in Iran. Korte and Kozur (2010) identified the onset of the shift as within the *Clarkina bachmanni* conodont zone, which is approximately correlative with the *Dzhulfites* beds (their Fig. 2). These assignments date the onset of the Late Permian C-isotopic shift to the early Changhsingian Stage. Since P–Tr boundary sections in China, Iran, and Europe have been rather well studied with regard to biostratigraphy, these differences in stratigraphic age between sections may be real, although further correlation studies will be required to substantiate this inference.

Richoz et al. (2010) inferred that the shift commenced ~2.2 Myr prior to the end-Permian marine mass extinction, whereas Korte and Kozur (2010) and Kozur (2007) estimated that it commenced only 0.45 to 0.50 Myr beforehand. Radiometric studies have shown that the duration of the Changhsingian Stage was about 3.5 Myr (Menning et al., 2006; Mundil et al., 2004, 2010). If sedimentation rates were uniform in a given P–Tr boundary section, then it would be a simple matter to convert thicknesses to time and determine the absolute age of the C-isotopic shift. For example, the duration of the pre-extinction negative shift in $\delta^{13}\text{C}_{\text{carb}}$ in South China would be about 0.1 Myr. However, stratigraphic correlation studies have demonstrated that many sections globally exhibit large (i.e., order-of-magnitude) changes in sedimentation rates through the P–Tr boundary interval (e.g., Algeo et al., 2007b, 2010; Algeo et al., submitted for publication-a), making application of this approach problematic. The Meishan D section, in particular, was characterized by condensed sedimentation around the time of the end-Permian event (Bowring et al., 1998, 1999; Yin et al., 2001) and, hence, the relative thicknesses of the Changhsingian Stage below (40 m) and above (2 m) the C-isotopic shift cannot be used to estimate its age of onset. Secular variations in sedimentation rates in the Iranian and European P–Tr boundary sections have not been determined, so age estimates based on an assumption of uniform sedimentation rates would be speculative. Thus, at present it cannot be definitively determined whether the onset of the Late Permian negative C-isotope excursion occurred 0.5 Myr (Korte and Kozur, 2010) or >2.0 Myr (Richoz et al., 2010) prior to the end-Permian mass extinction event.

5.3. Relationship of $\delta^{13}\text{C}_{\text{carb}}$ variation to the marine mass extinction event

The relationship of the negative $\delta^{13}\text{C}_{\text{carb}}$ shift in uppermost Permian strata (N1a–b) to the end-Permian mass extinction is a controversial

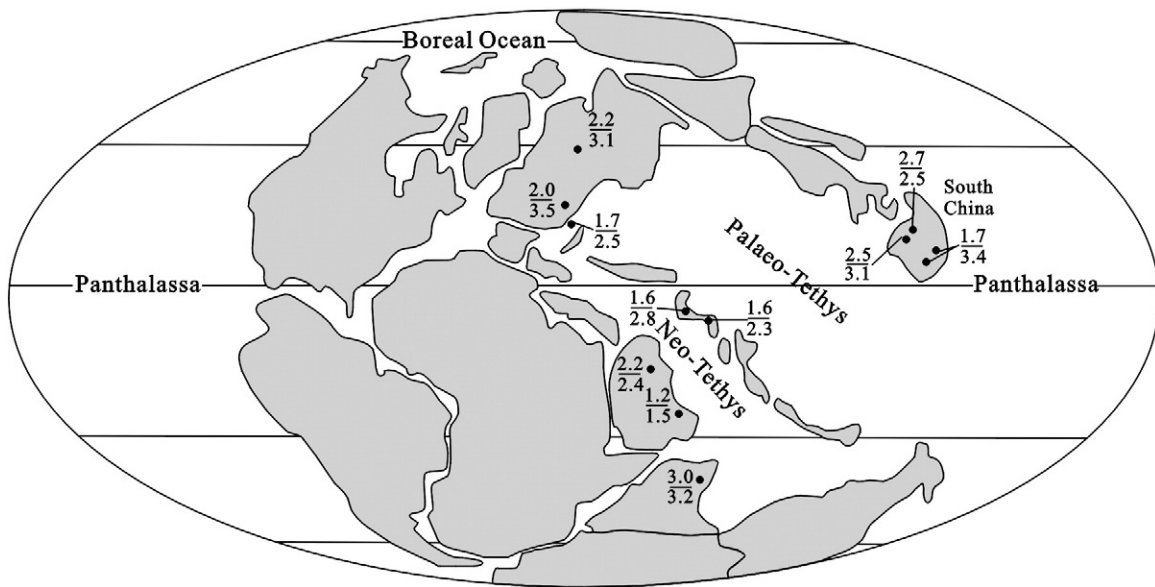


Fig. 9. Comparison between the magnitude of the pre-extinction and post-extinction negative shift in $\delta^{13}\text{C}_{\text{carb}}$ in sections around the Tethys Ocean. The denominator and numerator represent the magnitude of pre-extinction and post-extinction C-isotopic shifts, respectively. Sources of data are cited in the text.

subject. A key unresolved issue is whether the mass extinction induced the N1 C-isotopic shift or whether the mechanisms that caused end-Permian mass extinction also induced the N1 C-isotopic shift (Grard et al., 2005). Because the minimum value of $\delta^{13}\text{C}_{\text{carb}}$ in the PTCl (i.e., top of N1a interval) is always located above the main marine mass extinction horizon (Algeo et al., 2007a; Baud et al., 1989; Corsetti et al., 2005; Cao et al., 2002; Dolenc et al., 2001; Gorjan et al., 2008; Holser et al., 1989; Korte and Kozur, 2010; Korte et al., 2004; Krull et al., 2004; Payne et al., 2004; Xie et al., 2007; this study), it has been widely assumed that the mass extinction induced the N1 C-isotopic shift (Grard et al., 2005; Rampino and Caldeira, 2005; Wang et al., 1994). However, the magnitude of the post-extinction C-isotopic shift (N1a) is generally smaller ($\sim 1\text{--}2\%$) than that of the pre-extinction shifts (N1b + N2 $> 3\%$; Fig. 8). The same pattern is observed in other sections in South China as well as throughout the western Palaeo-Tethys and Neo-Tethys regions (Fig. 9). The small magnitude of the N1a C-isotopic shift indicates that the marine extinction event had at most a limited effect on the global carbon cycle and certainly could not have triggered the Upper Permian negative C-isotopic shift, which began well in advance of the mass extinction (Fig. 8). Furthermore, $\delta^{13}\text{C}_{\text{carb}}$ did not become more negative immediately after the main marine mass extinction—rather, it remained constant or shifted toward more positive values (Fig. 8). This counterintuitive phenomenon is observed in several sections and has been cited as evidence of continuous sedimentation through the crisis interval (Korte and Kozur, 2010; Richoz et al., 2010). This apparently global rebound toward more ^{13}C -enriched carbon isotope compositions directly after the end-Permian mass extinction may have been caused by one of the following mechanisms: (1) increased photosynthetic fractionation of carbon isotopes due to high atmospheric $p\text{CO}_2$ (Hayes et al., 1999; Kump and Arthur, 1999) or changes in the microbial communities (Luo et al., 2010; Riccardi et al., 2007); or (2) an increase in the organic carbon burial fraction (Kump and Arthur, 1999). At present, it is not possible to distinguish among these mechanisms. Clearly, other mechanisms must be considered to account for the negative shift in $\delta^{13}\text{C}_{\text{carb}}$ during the Late Permian—mechanisms that may also have been the trigger for the end-Permian mass extinction.

5.4. Causes of the pre-extinction negative shift in $\delta^{13}\text{C}_{\text{carb}}$

From the foregoing analysis, we may conclude that marine strata of the PTCl record a negative $\delta^{13}\text{C}_{\text{carb}}$ shift that took place in two steps

during the Late Permian to Early Triassic. Below, we review the primary mechanisms that may have caused these negative $\delta^{13}\text{C}_{\text{carb}}$ shifts and evaluate their probabilities based on characteristics of the C-isotope records of the present study.

5.4.1. Changes in marine primary productivity

One commonly proposed mechanism linking the end-Permian mass extinction event to the N1 C-isotopic shift is a severe reduction in marine primary and/or export productivity, producing a 'Strangelove ocean' similar to that existing after the end-Cretaceous mass extinction (Kump, 1991; Zachos et al., 1989). It should be emphasized that the end-Permian mass extinction event is a record primarily of changes in the diversity of the marine metazoan community—its effects on marine primary producers are not well understood, although studies have shown that eukaryotic algae were reduced in abundance relative to prokaryotes during this interval (Cao et al., 2009; Chen et al., in press; Grice et al., 2005; Luo et al., submitted for publication). The marine $\delta^{13}\text{C}_{\text{carb}}$ record is potentially a proxy for marine export productivity rates, changes in which generally induce changes in the burial flux of organic carbon and, hence, in the C-isotopic composition of seawater ΣCO_2 (Kump, 1991). Negative shifts in the marine $\delta^{13}\text{C}_{\text{carb}}$ record during the Late Permian may potentially reflect declines in marine primary productivity in advance of changes at higher trophic levels of marine ecosystems, or a collapse of the biological pump (reduction in export productivity, i.e., in the flux of organic matter out of the photic zone) resulting from a loss of zooplankton grazers producing fecal pellets or from other mechanisms of particle aggregation that promote settling. Complete collapse of biological productivity and cessation of organic matter burial is expected to yield $\delta^{13}\text{C}_{\text{carb}}$ values of $\sim -5\%$ for seawater ΣCO_2 and marine carbonates at timescales of a few hundred thousand years (Kump, 1991). However, recent work shows that no significant long-term productivity collapse occurred during the P–T transition. In fact, as evidenced by changes in organic carbon burial fluxes, productivity appears to have been enhanced in the earliest Triassic (Algeo et al., 2010; Algeo et al., submitted for publication-b; Wignall et al., 2010), probably due to an increased flux of nutrients to marine systems (Algeo et al., submitted for publication-c), leading to blooms of microbes favoring eutrophic conditions, such as acritarchs, prasinophytes, and cyanobacteria (Xie et al., 2010). As noted above, the shift toward more ^{13}C -enriched carbon isotopic compositions directly after

the end-Permian mass extinction could have been caused partly by an increase in the organic carbon burial fraction.

5.4.2. Eustatic regression

Eustatic regression, inducing loss of habitable area in epicontinental seas, has been imputed as a cause of marine mass extinctions at least since Newell (1967). However, subsequent research showed that the Late Permian global eustatic regression occurred prior to the mass extinction event (Hallam and Wignall, 1999; Yin et al., 2007). In the Meishan section, this regression was characterized by a type II sequence boundary at the base of bed 24e (Zhang et al., 1996). As sea-level dropped, large areas of lagoonal and continental shelf deposits containing relatively fresh organic matter were exposed to subaerial erosion. Oxidation of this ^{13}C -depleted organic matter may have caused a gradual negative shift in $\delta^{13}\text{C}_{\text{carb}}$, as proposed by Holser et al. (1989) and Faure et al. (1995). However, if erosion liberated organic carbon and carbonate carbon in the same proportion in which they were represented by the global riverine input prior to the sea-level fall, then the carbon isotopic composition of the flux carried to the ocean would not have changed significantly (Kump and Arthur, 1999) and thus would not have caused a negative isotope shift. On the other hand, even if the shallow-marine sediments undergoing erosion had had a higher ratio of organic carbon-to-carbonate than the global riverine average, mass balance considerations suggest that the carbon isotopic composition of the flux carried to the ocean should have been about -7.5% . In this case, the organic carbon oxidation flux would have to have been larger than $2.4 \times 10^{16} \text{ mol ka}^{-1}$ in order to achieve the negative C-isotope shift observed in Late Permian carbonates (Kump and Arthur, 1999). A flux of this magnitude is probably unrealistically large. Furthermore, the type 2 character of the sequence stratigraphy below bed 24e in the Meishan section (Zhang et al., 1996) implies that the end-Permian sea-level drop could not have been very large. Thus, sea-level regression alone was probably not a sufficient mechanism to account for more than a fraction of the negative shift in $\delta^{13}\text{C}_{\text{carb}}$ during the Late Permian.

5.4.3. Terrestrial crisis

A large quantity of organic matter of terrigenous origin has been buried in continental and marine sedimentary basins since the advent of higher land plants in the Devonian (Algeo et al., 1995). Broecker and Peacock (1999) argued that the negative shift in carbon isotopic composition of carbonate during the P–Tr transition could have been caused by the extinction of continental plants. Reduction of terrestrial ecosystem productivity and biomass would have reduced the burial flux of organic carbon from this source, contributing to the pre-extinction negative shift in marine $\delta^{13}\text{C}_{\text{carb}}$. Furthermore, deterioration of terrestrial ecosystems is likely to have led to soil erosion, increasing the oxidation rate of soil organic matter, which would have introduced abundant, ^{13}C -depleted carbon into the ocean (Algeo et al., submitted for publication-b,c). Studies of terrestrial successions have shown that there was a major turnover in terrestrial floras during the PTCI, when mature gymnosperm-dominated floras yielded to rapidly growing early successional communities dominated by lycopsids and ferns (Looy et al., 1999, 2001), and that this process was accompanied by major changes in clastic sediment production and transport (Algeo et al., submitted for publication-a; Michaelsen, 2002; Retallack, 2005; Ward et al., 2000). Study of lipid biomarkers in marine successions has shown that the signature of soil erosion appeared in the marine record just prior to the end-Permian marine mass extinction horizon (Luo et al., submitted for publication; Sephton et al., 2005; Watson et al., 2005; Wang, 2007; Wang and Visscher, 2007; Xie et al., 2007). Large quantities of volcanic dust and sulphate aerosols released into the atmosphere are thought to have caused global cooling and acid rain (cf. Self et al., 2008), which would have killed terrestrial life quickly and potentially contributed to the negative C-isotopic shift in marine carbonates during the Late Permian.

5.4.4. Volcanism

The volcanic activity of the Siberian Traps may have been a direct influence on the marine mass extinction and $\delta^{13}\text{C}_{\text{carb}}$ record, either through release of volcanic CO_2 (Payne and Kump, 2007) or through generation of thermogenic CO_2 and methane as magma was intruded into the West Siberian coal fields (Korte et al., 2010; Kamo et al., 2003; Retallack and Jahren, 2008; Reichow et al., 2009; Svensen et al., 2009). However, the main stage of the Siberian Traps eruptions was probably later than the pre-extinction stepwise decline in $\delta^{13}\text{C}_{\text{carb}}$ recorded in the skeletal limestones of the four sections of the present study (Saunders and Reichow, 2009; Xie et al., 2010 and references therein). In the Taiping section, there are at least two white grey ash beds in the upper part of the skeletal limestone (Fig. 3) that are of volcanic origin (Lehrmann et al., 2003). There are also several ash beds in the upper Dalong Formation (Late Changhsingian) of the Dongpan section, a deep-water succession near the Taiping and Zuodeng sections (Meng et al., 2005). These ash beds are evidence that felsic volcanism began at least by Late Changhsingian time in South China. As mentioned above, the stepwise decline in $\delta^{13}\text{C}_{\text{carb}}$ presented in the four sections seems to be caused by the episodic volcanism eruption which may also induces episodic variation in other issues, such as terrestrial crisis and continental weathering (Xie et al., 2007). The strength of this episodic volcanism would be too weak or too local to induce global marine mass extinction but might have been sufficient to disrupt terrestrial ecosystems which exposes to the atmosphere directly and initiate soil erosion, a process that potentially could have produced a negative shift in the marine $\delta^{13}\text{C}_{\text{carb}}$ record prior to the end-Permian extinction event. In addition, PTB volcanic activity was widespread along the western Panthalassa margin and Gondwanaland, and these volcanism eruptions outside South China could have contributed to the observed shift in $\delta^{13}\text{C}_{\text{carb}}$.

5.4.5. Biogenic methane release

Biogenic methane is significantly depleted in ^{13}C , with $\delta^{13}\text{C}$ typically -30% to -80% (Holser et al., 1988), making it an oft-invoked mechanism for large negative shifts in the marine $\delta^{13}\text{C}_{\text{carb}}$ record, such as that accompanying the PETM (Palaeocene–Eocene Thermal Maximum) (Zeebe et al., 2009). The negative shift in $\delta^{13}\text{C}_{\text{carb}}$ during the P–Tr transition has also been ascribed to fossil methane release (Berner, 2002; Erwin, 1993; Krull and Retallack, 2000; Krull et al., 2000, 2004). The two largest potential sources of fossil biogenic methane are (1) methane clathrates found in continental shelf sediments, (2) production of methane during melting of high-latitude permafrost (Kvenvolden and Rogers, 2005). Recently, Luo et al. (submitted for publication) showed that oceanic sulphate concentrations were very low during the PTCI. Because sulphate is an important electron acceptor during anaerobic methane oxidation (Valentine, 2002), its near-absence in Late Permian seawater would have allowed any methane released from seafloor clathrates to have escaped into the atmosphere. However, there is no firm evidence to support a massive release of methane during the PTCI other than the marine $\delta^{13}\text{C}_{\text{carb}}$ record, which (as shown here) allows multiple interpretations. The modeling results of Berner (2002) were based on a diagenetically influenced $\delta^{13}\text{C}_{\text{carb}}$ profile from the Meishan section, and the latitudinal gradient in $\delta^{13}\text{C}_{\text{carb}}$ reported by Krull et al. (2000) is questionable owing to local effects on organic carbon isotope compositions as well as diagenetic influences (Erwin et al., 2002; Mii et al., 1997). Thus, it is unclear whether methane release played any significant role in the negative Late Permian C-isotopic shift.

In summary, marine C-isotopic records probably cannot resolve the debate concerning the origin of the negative shifts in $\delta^{13}\text{C}_{\text{carb}}$ during the Late Permian. The $\delta^{13}\text{C}_{\text{carb}}$ results presented here suggest that episodic volcanism, probably in combination with deterioration of terrestrial ecosystems, soil erosion, and decreased marine primary or export productivity, is a likely cause of the C-isotopic shifts. However, more compelling evidence to support this inference will have to await studies that constrain process through demonstrating

significant patterns of covariation between marine $\delta^{13}\text{C}_{\text{carb}}$ and other records of changes in the biota, environments, and sediments of the PTCI.

6. Conclusions

High-resolution marine $\delta^{13}\text{C}_{\text{carb}}$ profiles were analyzed in four P–Tr boundary sections with microbialite from South China. Isotopic and elemental evidence indicate that these sections preserve primary records of marine carbonate C-isotopic variation. No distinct difference in $\delta^{13}\text{C}_{\text{carb}}$ exists between the microbialite and coeval non-microbialite samples. The profiles of $\delta^{13}\text{C}_{\text{carb}}$ in the PTCI in the four sections are characterized by a large and stepwise negative shift through the Upper Permian, indicating a distinct perturbation to the global carbon cycle prior to the end-Permian marine biotic crisis. The magnitude of the pre-extinction negative shift in $\delta^{13}\text{C}_{\text{carb}}$ is much larger than that of the post-extinction shift, indicating that the extinction event was not the primary cause of changes in the global carbon cycle. Rather, the pre-extinction stepwise negative shift in $\delta^{13}\text{C}_{\text{carb}}$ is likely to have been caused by episodic activity of volcanic system, leading to deterioration of terrestrial ecosystems and soil erosion, although the influence of eustatic regression and biogenic methane release cannot be entirely ruled out. The aftereffects of these processes would have been the direct cause of the end-Permian mass extinction.

Acknowledgments

We have to send our sincere thanks to Prof. Hongfu Yin for his comments on the earlier manuscript. Master student Wei Liao and Jianbo Chen in CUG are thanked here for their help during the samples' collection and preparation. We express our thanks to David Bottjer and two anonymous reviewers for their constructive comments that greatly improved the quality of this paper. This work was supported by the 973 program (Grant no. 2011CB808800), the Chinese National Natural Science Foundation (Grant nos. 40730209, 40921062, 40930210, and 41002003), and the 111 project (B08030) and by grants from the U.S. National Science Foundation to Algeo (EAR-0745574) and Kump (EAR-0707461). This paper is a contribution to IGCP Project 572.

References

- Algeo, T.J., Wilkinson, B.H., Lohmann, K.C., 1992. Meteoric-burial diagenesis of Pennsylvanian carbonate: water/rock interactions and basin geothermics. *Journal of Sedimentary Petrology* 62, 652–670.
- Algeo, T.J., Berner, R.A., Maynard, J.B., Scheckler, S.T., 1995. Late Devonian oceanic anoxic events and biotic crises: "rooted" in the evolution of vascular land plants? *GSA Today* 5, 63–66.
- Algeo, T.J., Ellwood, B., Nguyen, T.K.T., Rowe, H., Maynard, J.B., 2007a. The Permian–Triassic boundary at Nhi Tao, Vietnam: evidence for recurrent influx of sulfidic watermasses to a shallow-marine carbonate platform. *Palaeogeography, Palaeoclimatology, Palaeoecology* 252 (1–2), 304–327.
- Algeo, T.J., Hannigan, R., Rowe, H., Brookfield, M., Baud, A., Krystyn, L., Ellwood, B.B., 2007b. Sequencing events across the Permian–Triassic boundary, Guryul Ravine (Kashmir, India). *Palaeogeography, Palaeoclimatology, Palaeoecology* 252, 328–346.
- Algeo, T.J., Hinnov, L., Moser, J., Maynard, J.B., Elswick, E.E., Kuwahara, K., Sano, H., 2010. Changes in productivity and redox conditions in the Panthalassic Ocean during the latest Permian. *Geology* 38, 187–190.
- Algeo, T.J., Henderson, C., Ellwood, B.B., Rowe, H., Elswick, E.E., Bates, S., Lyons, T., Hower, J.C., Smith, C., Maynard, J.B., Hays, L., Summons, R., Fulton, J., Freeman, K., submitted for publication-a. Elevated sediment fluxes at a high northern paleolatitute site prior to the latest Permian event horizon: link to Siberian Traps volcanism? *Geological Society of America Bulletin*, submitted August 2010.
- Algeo, T.J., Henderson, C.M., Tong, J., Feng, Q., Yin, H., and Tyson, R., submitted for publication-b. Plankton and productivity at the Permian–Triassic boundary: an analysis of organic carbon fluxes. *Global and Planetary Change*, submitted September 2010.
- Algeo, T.J., Chen, Z.Q., Fraiser, M.L., Twitchett, R.J., submitted for publication-c. Terrestrial-marine teleconnections in the collapse and rebuilding of Early Triassic marine ecosystems. *Palaeogeography, Palaeoclimatology, Palaeoecology*, submitted September 2010.
- Basu, A.R., Petaev, M.I., Poreda, R.J., Jacobsen, S.B., Becker, L., 2003. Chondritic meteorite fragments associated with the Permian–Triassic boundary in Antarctica. *Science* 302, 1388–1392.
- Baud, A., Magaritz, M., Holser, W.T., 1989. Permian–Triassic of the Tethys: carbon isotope studies. *Geologische Rundschau* 78, 649–677.
- Baud, A., Richoz, S., Pruss, S., 2007. The lower Triassic anachronistic carbonate facies in space and time. *Global and Planetary Change* 55, 81–89.
- Becker, L., Poreda, R.J., Basu, A.R., Pope, K.O., Harrison, T.M., Nicholson, C., Iasky, R., 2004. Bedout: a possible end-Permian impact crater offshore of Northwestern Australia. *Science* 304, 1469–1476.
- Berner, R.A., 2002. Examination of hypotheses for the Permo-Triassic boundary extinction by carbon cycle modeling. *Proceedings of the National Academy of Sciences of the United States of America* 99, 4172–4177.
- Bottjer, D.J., Clapham, M.E., Fraiser, M.L., Powers, C.M., 2008. Understanding mechanisms for the end-Permian mass extinction and the protracted Early Triassic aftermath and recovery. *GSA Today* 18, 4–10.
- Bowring, S.A., Erwin, D.H., Jin, Y.G., Martin, M.W., Davidek, K., Wang, W., 1998. U/Pb zircon geochronology and tempo of the end-Permian mass extinction. *Science* 280, 1039–1045.
- Bowring, S.A., Erwin, D.H., Isozaki, Y., 1999. The tempo of mass extinction and recovery: the end-Permian example. *Proceedings of the National Academy of Sciences of the United States of America* 96, 8827–8828.
- Broecker, W.S., Peacock, S., 1999. An ecologic explanation for the Permo-Triassic carbon and sulfur isotope shifts. *Global Biogeochemical Cycles* 13, 1167–1172.
- Cao, C.Q., Wang, W., Jin, Y.G., 2002. The change of carbon isotope during the Permian–Triassic boundary in Meishan, Zhejiang province. *Chinese Science Bulletin* 47, 302–306.
- Cao, C.Q., Love, G.D., Hays, L.E., Wang, W., Shen, S.Z., Summons, R.E., 2009. Biogeochemical evidence for euxinic oceans and ecological disturbance presaging the end-Permian mass extinction event. *Earth and Planetary Science Letters* 281, 188–201.
- Chen, J., Beatty, T.W., Henderson, C.M., Rowe, H., 2009. Conodont biostratigraphy across the Permian–Triassic boundary at the Dawen section, Great Bank of Guizhou, Guizhou Province, South China: implications for the Late Permian extinction and correlation with Meishan. *Journal of Asian Earth Sciences* 36, 442–458.
- Chen, L., Wang, Y., Xie, S., Kershaw, S., Dong, M., Yang, H., Liu, H., Algeo, T.J., in press. Molecular records of microbialites following the end-Permian mass extinction in Chongyang, Hubei Province, South China. *Palaeogeography Palaeoclimatology Palaeoecology*.
- Collin, P.Y., Kershaw, S., Crasquin-Soleau, S., Feng, Q.L., 2009. Facies changes and diagenetic processes across the Permian–Triassic boundary event horizon, Great Bank of Guizhou, South China: a controversy of erosion and dissolution. *Sedimentology* 56, 677–693.
- Corsetti, F.A., Baud, A., Marengo, P.J., Richoz, S., 2005. Summary of Early Triassic carbon isotope records. *Comptes Rendus Palevol* 4, 473–486.
- Cui, Y., Liu, J.B., Ezaki, Y., 2008. Fluctuations of stable carbon isotopes around the Permian–Triassic boundary in Huaying of Sichuan, South China: its characteristics and biogeochemical origin. *Acta Scientiarum Naturalium Universitatis Pekinensis* 3, 95–105.
- Dolenc, T., Lojen, S., Ramovs, A., 2001. The Permian–Triassic boundary in Western Slovenia (Idrija Valley section): magnetostratigraphy, stable isotopes, and elemental variations. *Chemical Geology* 175, 175–190.
- Erwin, D.H., 1993. *The Great Paleozoic Crisis. Life and Death in the Permian*. Columbia University press, New York. 327 pp.
- Erwin, D.H., Bowring, S.A., Jin, Y.G., 2002. End-Permian mass extinctions: a review. *Boulder Geological Society of America Special Paper* 356, 363–384.
- Faure, K., de Wit, M.J., Willis, J.P., 1995. Late Permian global coal hiatus linked to 13C-depleted CO₂ flux into the atmosphere during the final consolidation of Pangea. *Geology* 23, 507–510.
- Feng, Z.Z., Yang, Y.Q., Jin, Z.K., Li, S.W., Bao, Z.D., 1997. Lithofacies Palaeogeography of Permian of South China. *Petroleum University Press, Beijing*. 1–242pp.
- Gorjan, P., Kaiho, K., Chen, Z.Q., 2008. A carbon-isotopic study of an end-Permian mass extinction horizon, Bulla, Northern Italy: a negative $\delta^{13}\text{C}$ shift prior to the marine extinction. *Terra Nova* 20, 253–258.
- Grard, A., François, L.M., Dessert, C., Dupré, B., Goddérès, Y., 2005. Basaltic volcanism and mass extinction at the Permo-Triassic boundary: environmental impact and modeling of the global carbon cycle. *Earth and Planetary Science Letters* 234, 207–221.
- Grice, K., Cao, C.Q., Love, G.D., Böttcher, M.E., Twitchett, R.J., Grosjean, E., Summons, R.E., Turgeon, S.C., Dunning, W., Jin, Y.G., 2005. Photoc zone euxinia during the Permian–Triassic superanoxic event. *Science* 307, 706–709.
- Haas, J., Demény, A., Hips, K., Zajzon, N., Weiszburg, T.G., Sudar, M., Pálffy, J., 2007. Biotic and environmental changes in the Permian–Triassic boundary interval recorded on a western Tethyan ramp in the Bukk Mountains, Hungary. *Global and Planetary Change* 55, 136–154.
- Hallam, A., Wignall, P.B., 1999. Mass extinctions and sea-level changes. *Earth Science Reviews* 48, 217–250.
- Hayes, J.M., Strauss, H., Kaufman, A.J., 1999. The abundance of ^{13}C in marine organic matter and isotopic fractionation in the global biogeochemical cycle of carbon during the past 800 Ma. *Chemical Geology* 161, 103–125.
- He, W.H., Shi, G.R., Feng, Q.L., Campi, M.J., Gu, S.Z., Bu, J.J., Peng, Y.Q., Meng, Y.Y., 2007. Brachiopod miniaturization and its possible causes during the Permian–Triassic crisis in deep water environments, South China. *Palaeogeography, Palaeoclimatology, Palaeoecology* 252, 145–163.
- Holser, W.T., Schidlowski, M., Mackenzie, F.T., Maynard, J.B., 1988. Geochemical cycles of carbon and sulfur. In: Gregor, C.B., Garrels, R.M., Mackenzie, F.T., Maynard, J.B. (Eds.), *Chemical Cycles in the Evolution of the Earth*. Wiley, New York, pp. 105–173.

- Holser, W.T., Schonlaub, H.-P., Attrep Jr., M., Boeckelmann, K., Klein, P., Magaritz, M., Orth, C.J., Fenninger, A., Jenny, C., Kralik, M., Mauritsch, H., Pak, E., Schramm, J.-M., Statterger, K., Schmoller, R., 1989. A unique geochemical record at the Permian–Triassic boundary. *Nature* 337, 39–44.
- Irwin, H., Curtis, C., Coleman, M., 1977. Isotopic evidence for source of diagenetic carbonates formed during burial of organic-rich sediments. *Nature* 269, 209–213.
- Isozaki, Y., 1997. Permo-Triassic superanoxia and stratified superocean: records from lost deep sea. *Science* 276, 235–238.
- Jiang, H.S., Lai, X.L., Luo, G.M., Aldridge, R.J., Zhang, K.X., Wignall, P., 2007. Restudy of conodont zonation and evolution across the Permian–Triassic Boundary at Meishan Section, Changxing, Zhejiang. *Global and Planetary Change* 55, 39–55.
- Kamo, S.L., Czamanske, G.K., Amelin, Y., Fedorenko, V.A., Davis, D.W., Trofimov, V.R., 2003. Rapid eruption of Siberian flood-volcanic rocks and evidence for coincidence with the Permian–Triassic boundary and mass extinction at 251 Ma. *Earth and Planetary Science Letters* 214, 75–91.
- Kaufman, A.J., Knoll, A.H., 1995. Neoproterozoic variations in the C-isotopic composition of seawater: stratigraphic and biogeochemical implications. *Precambrian Research* 73, 27–49.
- Knoll, A.H., Bambach, R.K., Canfield, D.E., Grotzinger, J.P., 1996. Comparative earth history and Late Permian mass extinction. *Science* 273, 452–457.
- Knoll, A.H., Bambach, R.K., Payne, J.L., Pruss, S.B., Fischer, F., 2007. Paleophysiology and end-Permian mass extinction. *Earth and Planetary Science Letters* 256, 295–313.
- Korte, C., Kozur, H., 2005. Carbon isotope stratigraphy across the Permian–Triassic boundary at Jolfa (NW Iran), Peitlerkofel (Sas de Putia, Sass de Putia), Pufels (Bula, Bulla), Tesero (all three Southern Alps, Italy) and Gerennavár (Bükk Mts., Hungary). *Journal of Alpine Geology* 47, 119–135.
- Korte, C., Kozur, H.W., 2010. Carbon isotope stratigraphy across the Permian–Triassic boundary: a review. *Journal of Asian Earth Sciences* 39, 215–235.
- Korte, C., Kozur, H.W., Joachimski, M.M., Strauss, H., Veizer, J., Schwark, L., 2004. Carbon, sulfur, oxygen and strontium isotope records, organic geochemistry and biostratigraphy across the Permian/Triassic boundary in Abadeh, Iran. *International Journal of Earth Sciences* 93, 565–581.
- Korte, C., Jasper, T., Kozur, H.W., Veizer, J., 2005. $\delta^{18}\text{O}$ and $\delta^{13}\text{C}$ of Permian brachiopods: a record of seawater evolution and continental glaciation. *Palaeogeography, Palaeoclimatology, Palaeoecology* 224, 333–351.
- Korte, C., Pande, P., Kalia, P., Kozur, H., Joachimski, M.M., Oberhansli, H., 2010. Massive volcanism at the Permian–Triassic boundary and its impact on the isotopic composition of the ocean and atmosphere. *Journal of Asian Earth Sciences* 37, 293–311.
- Kozur, H.W., 2007. Biostratigraphy and event stratigraphy in Iran around the Permian–Triassic Boundary (PTB): implications for the causes of the PTB biotic crisis. *Global and Planetary Change* 55, 155–176.
- Krull, E.S., Retallack, G.J., 2000. $\delta^{13}\text{C}$ depth profiles from paleosols across the Permian–Triassic boundary: evidence for methane release. *GSA Bulletin* 112, 1459–1472.
- Krull, E.S., Retallack, G.J., Campbell, I.H., Lyon, G.L., 2000. $\delta^{13}\text{C}$ Corg chemostratigraphy of the Permian–Triassic boundary in the Maitai Group, New Zealand: evidence for high-latitude methane release. *New Zealand Journal of Geology and Geophysics* 43, 21–32.
- Krull, E.S., Lehrmann, D.J., Druke, D., Kessel, B., Yu, Y.Y., Li, R.X., 2004. Stable carbon isotope stratigraphy across the Permian–Triassic boundary in shallow marine carbonate platforms, Nanpanjiang Basin, south China. *Palaeogeography, Palaeoclimatology, Palaeoecology* 204, 297–315.
- Kump, L.R., 1991. Interpreting carbon-isotope excursions: Strangelove oceans. *Geology* 19, 299–302.
- Kump, L.R., Arthur, M.A., 1999. Interpreting carbon-isotope excursions: carbonates and organic matter. *Chemical Geology* 161, 181–198.
- Kump, L.R., Pavlov, A., Arthur, M.A., 2005. Massive release of hydrogen sulfide to the surface ocean and atmosphere during interval of oceanic anoxia. *Geology* 33, 397–400.
- Kvenvolden, K.A., Rogers, B.W., 2005. Gaia's breath—global methane exhalations. *Marine and Petroleum Geology* 22, 579–590.
- Lehrmann, D.J., 1999. Early Triassic calcimicrobial mounds and biostromes of the Nanpanjiang basin, South China. *Geology* 27, 359–362.
- Lehrmann, D.J., Payne, J.L., Felix, S.V., Dillett, P.M., Wang, H.M., Yu, Y.Y., Wei, J.Y., 2003. Permian–Triassic boundary sections from shallow-marine carbonate platforms of the Nanpanjiang Basin, South China: implications for oceanic conditions associated with the End-Permian extinction and its aftermath. *Palaios* 18, 138–152.
- Lehrmann, D.J., Ramezani, J., Bowring, S.A., Martin, M.W., Montgomery, P., Enos, P., Payne, J.L., Orchard, M.J., Wang, H.M., Wei, J.Y., 2006. Timing of recovery from the end-Permian extinction: geochronologic and biostratigraphic constraints from south China. *Geology* 34, 1053–1056.
- Liu, J.B., Ezaki, Y., Yang, S.R., Wang, H.F., Adachi, N., 2007. Age and sedimentology of microbialites after the end-Permian mass extinction in Luodian, Guizhou Province. *Journal of Palaeogeography* 9, 473–486 (in Chinese with English abstract).
- Looy, C.V., Brugman, W.A., Dilcher, D.L., Visscher, H., 1999. The delayed resurgence of equatorial forests after the Permian–Triassic ecological crisis. *Proceedings of the National Academy of Sciences of the United States of America* 96, 13857–13862.
- Looy, C.V., Twitcheit, R.J., Dilcher, D.L., van Konijnenburg-van Cittert, J.H.A., Visscher, H., 2001. Life in the end-Permian dead zone. *Proceedings of the National Academy of Sciences of the United States of America* 98, 7879–7883.
- Luo, G.M., Lai, X.L., Jiang, H.S., Zhang, K.X., 2006. Size variation of the end Permian conodont Neogondolella at Meishan Section, Changxing, Zhejiang and its significance. *Science in China Series D* 49, 337–347.
- Luo, G.M., Lai, X.L., Shi, G.R., Jiang, H.S., Yin, H.F., Xie, S.C., Tong, J.N., Zhang, K.X., He, W.H., Wignall, P.B., 2008. Size variation of conodont elements of the Hindeodus-Isarcicella clade during the Permian–Triassic transition in South China and its implication for mass extinction. *Palaeogeography, Palaeoclimatology, Palaeoecology* 264, 176–187.
- Luo, G.M., Huang, J.H., Xie, S.C., Wignall, P.B., Tang, X.Y., Huang, X.Y., Yin, H.F., 2010. Relationships between carbon isotope evolution and variation of biota during the Permian–Triassic transition at Meishan Section, South China. *International Journal of Earth Sciences* 99, 775–784.
- Luo, G.M., Kump, L.R., Wang, Y.B., Tong, J.N., Arthur, M.A., Yang, H., Huang, J.H., Yin, H.F., Xie, S.C., 2010. Isotopic evidence for an anomalously low oceanic sulphate concentration following end-Permian mass extinction. *Earth and Planetary Science Letters* 300 (1–2), 101–111.
- Luo, G.M., Wang, Y.B., Grice, K., Kershaw, S., Ruan, X.Y., Yang, H., Jia, C.L., Xie, S.C., submitted for publication. Microbial composition in microbialites during the Late Permian ecological crisis in the Cili section, South China: Evidence from lipid biomarkers. *Applied Geochemistry*.
- Marshall, J.D., 1992. Climatic and oceanographic isotopic signals from the carbonate rock record and their preservation. *Geological Magazine* 129, 143–160.
- McCrea, J.M., 1950. The isotopic chemistry of carbonates and a paleotemperature scale. *The Journal of Chemical Physics* 18, 849–857.
- Meng, Y.Y., Feng, Q.L., He, W.H., Gu, S.Z., Jin, Y.X., Zhang, F., 2005. A unique deep-water Permian–Triassic boundary section from the Liujiao region in Southwestern Guangxi, South China. *Journal of Stratigraphy* 29, 323–332 (In Chinese with English abstract).
- Menning, M., Alekseev, A.S., Chuvashov, B.I., Davydov, V.I., Devuyt, F.X., Forke, H.C., Grunt, T.A., Hance, L., Heckel, P.H., Izokh, N.G., Jin, Y.G., Jones, P.J., Kotlyar, G.V., Kozur, H.W., Nemyrovska, T.I., Schneider, J.W., Wang, X.D., Weddige, K., Weyer, D., Work, D.M., 2006. Global time scale and regional stratigraphic reference scales of Central and West Europe, East Europe, Tethys, South China, and North America as used in the Devonian–Carboniferous–Permian Correlation Chart 2003 (DCP 2003). *Palaeogeography, Palaeoclimatology, Palaeoecology* 240 (1–2), 318–372.
- Meyer, K.M., Kump, L.R., Ridgwell, A., 2008. Biogeochemical controls on photic-zone euxinia during the end-Permian mass extinction. *Geology* 36, 747–750.
- Michaelsen, P., 2002. Mass extinction of peat-forming plants and the effect on fluvial styles across the Permian–Triassic boundary, northern Bowen Basin, Australia. *Palaeogeography, Palaeoclimatology, Palaeoecology* 179, 173–188.
- Mii, H.S., Grossman, E.L., Yancey, T.E., 1997. Stable carbon and oxygen isotope shifts in Permian seas of West Spitsbergen—global change or diagenetic artifact? *Geology* 25, 227–230.
- Mu, X.N., Kershaw, S., Li, Y., Guo, L., Qi, Y.P., Reynolds, A., 2009. High-resolution carbon isotope changes in the Permian–Triassic boundary interval, Chongqing, South China: implications for control and growth of earliest Triassic microbialites. *Journal of Asian Earth Sciences* 36, 434–441.
- Mundil, R., Ludwig, K.R., Metcalfe, I., Renne, P.R., 2004. Age and timing of the Permian mass extinction: U/Pb dating of closed-system zircons. *Science* 305, 1760–1763.
- Mundil, R., Pálffy, J., Renne, P.R., Brack, P., 2010. The Triassic time scale: new constraints and a review of geochronological data. *Geological Society of London* 334, 41–60.
- Nan, J.Y., Liu, Y.Y., 2004. Organic and inorganic carbon-isotope shift and paleoenvironment at the P–T boundary section in Meishan, Zhejiang Province. *Geochimica* 33, 9–19 (In Chinese with English abstract).
- Newell, N.D., 1967. Revolutions in the history life. *Geological Society of America Special Paper* 89, 63–91.
- Payne, J.L., Kump, L.R., 2007. Evidence for recurrent Early Triassic massive volcanism from quantitative interpretation of carbon isotope fluctuations. *Earth and Planetary Science Letters* 256, 264–277.
- Payne, J.L., Lehrmann, D.J., Wei, J.Y., Orchard, M.J., Schrag, D.P., Knoll, A.H., 2004. Large perturbations of the carbon cycle during recovery from the End-Permian extinction. *Science* 305, 506–509.
- Payne, J.L., Lehrmann, D.J., Follett, D., Seibel, M., Kump, L.R., Riccardi, A.L., Altiner, D., Sano, H., Wei, J.Y., 2007. Erosional truncation of uppermost Permian shallow-marine carbonates and implications for Permian–Triassic boundary events. *Geological Society of America Bulletin* 119, 771–784.
- Pruss, S.B., Bottjer, D.J., Corsetti, F.A., Baud, A., 2006. A global marine sedimentary response to the end-Permian mass extinction: examples from southern Turkey and the western United States. *Earth Science Reviews* 78, 193–206.
- Rampino, M.R., Caldeira, K., 2005. Major perturbation of ocean chemistry and a “Strangelove Ocean” after the end-Permian mass extinction. *Terra Nova* 17, 554–559.
- Raup, D.M., Sepkoski, J.J., 1982. Mass extinction in the marine fossil record. *Science* 215, 1501–1503.
- Reichow, M.K., Pringle, M.S., Al'Mukhamedov, A.I., Allen, M.B., Andreichev, V.L., Buslov, M.M., Davies, C.E., Fedoseev, G.S., Fitton, J.G., Inger, S., Medvedev, A.Y., Mitchell, C., Puchkov, V.N., Safonova, I.Y., Scott, R.A., Saunders, A.D., 2009. The timing and extent of the eruption of the Siberian Traps large igneous province: implications for the end-Permian environmental crisis. *Earth and Planetary Science Letters* 277, 9–20.
- Renne, P.R., Black, M.T., Zhang, Z.C., Richards, M.A., Basu, A.R., 1995. Synchrony and causal relations between Permian–Triassic boundary crises and Siberian Flood volcanism. *Science* 269, 1413–1416.
- Retallack, G.J., 2005. Earliest Triassic claystone breccias and soil-erosion crisis. *Journal of Sedimentary Research* 75, 679–695.
- Retallack, G.J., Jahren, A.H., 2008. Methane release from igneous intrusion of coal during Late Permian extinction events. *Journal of Geology* 116, 1–20.
- Riccardi, A., Kump, L.R., Arthur, M.A., D'Hondt, S., 2007. Carbon isotopic evidence for chemocline upward excursions during the end-Permian event. *Palaeogeography, Palaeoclimatology, Palaeoecology* 248, 73–81.
- Richo, S., Krystyn, L., Baud, A., Brandner, R., Horacek, M., Mohtat-Aghai, P., 2010. Permian–Triassic boundary interval in the Middle East (Iran and N. Oman): progressive environmental change from detailed carbonate carbon isotope marine curve and sedimentary evolution. *Journal of Asian Earth Sciences* 39, 236–253.
- Saunders, A.D., Reichow, M.K., 2009. The Siberian Traps and the End-Permian mass extinction: a critical review. *Chinese Science Bulletin* 54, 20–37.

- Scholle, P.A., Arthur, M.A., 1980. Carbon isotope fluctuations in Cretaceous pelagic limestones: potential stratigraphic and petroleum exploration tool. *American Association of Petroleum Geologists Bulletin* 64, 67–87.
- Self, S., Blake, S., Sharma, K., Widdowson, M., Sephton, S., 2008. Sulfur and chlorine in Late Cretaceous Deccan magmas and eruptive gas release. *Science* 319, 1654–1657.
- Sephton, M.A., Looy, C.V., Brinkhuis, H., Wignall, P.B., de Leeuw, J.W., Visscher, H., 2005. Catastrophic soil erosion during the end-Permian biotic crisis. *Geology* 33, 941–944.
- Sepkoski Jr., J.J., 1989. Periodicity in extinction and the problem of catastrophism in the history of life. *Journal of the Geological Society of London* 146, 7–19.
- Svensen, H., Planke, S., Polozov, A.G., Schmidbauer, N., Corfu, F., Podladchikov, Y.Y., Jamtveit, B., 2009. Siberian gas venting and the end-Permian environmental crisis. *Earth and Planetary Science Letters* 277, 490–500.
- Twitchett, R.T., 2007. The Lilliput effect in the aftermath of the end-Permian extinction event. *Palaeogeography, Palaeoclimatology, Palaeoecology* 252, 132–144.
- Twitchett, R.J., Looy, C.V., Morante, R., Visscher, H., Wignall, P.B., 2001. Rapid and synchronous collapse of marine and terrestrial ecosystems during the end-Permian biotic crisis. *Geology* 29, 351–354.
- Valentine, D.L., 2002. Biogeochemistry and microbial ecology of methane oxidation in anoxic environments: a review. *Antonie van Leeuwenhoek* 81, 271–282.
- Wang, C.J., 2007. Anomalous hopane distributions at the Permian–Triassic boundary, Meishan, China—evidence for the end-Permian marine ecosystem collapse. *Organic Geochemistry* 38, 52–66.
- Wang, C.J., Visscher, H., 2007. Abundance anomalies of aromatic biomarkers in the Permian–Triassic boundary section at Meishan, China—evidence of end-Permian terrestrial ecosystem collapse. *Palaeogeography, Palaeoclimatology, Palaeoecology* 252, 291–303.
- Wang, K., Geldsetzer, H.H.J., Krouse, H.R., 1994. Permian–Triassic extinction: organic $\delta^{13}\text{C}$ evidence from British Columbia, Canada. *Geology* 22, 580–584.
- Wang, X., Hao, W., Yang, S., Liu, J., 1999. Stratigraphy and fusulinid fossils of the Upper Permian in Pingguo area, Guangxi. In: Yao, A., Ezaki, Y., Hao, W., Wang, X. (Eds.), *Biotic and Geological Developments in the Paleo-Tethys in China*. Peking University Press, Beijing, pp. 55–62.
- Wang, Y.B., Tong, J.N., Wang, J.S., Zhou, X.G., 2005. Calcimicrobialite after end-Permian mass extinction in South China and its palaeoenvironmental significance. *Chinese Science Bulletin* 50, 665–671.
- Wang, W., Kano, A., Okumura, T., Ma, Y., Matsumoto, R., Matsuda, N., Ueno, K., Chen, X., Kakuwa, Y., Gharai, M.H.M., Ilkhchi, M.R., 2007. Isotopic chemostratigraphy of the microbialite-bearing Permian–Triassic boundary section in the Zagros Mountains, Iran. *Chemical Geology* 244 (3–4), 708–714.
- Wang, Q.X., Tong, J.N., Song, H.J., Yang, H., 2009. Evolution of the ecosystem across the Permian–Triassic boundary at the Kangjiaping Section in Cili, Hunan Province. *Science in China Series D* 52, 797–806.
- Ward, P.D., Montgomery, D.R., Smith, R., 2000. Altered river morphology in South Africa related to the Permian–Triassic extinction. *Science* 289, 1740–1743.
- Watson, J.S., Sephton, M.A., Looy, C.V., Gilmour, I., 2005. Oxygen-containing aromatic compounds in a Late Permian sediment. *Organic Geochemistry* 36, 371–384.
- Wignall, P.B., Twitchett, R.J., 1996. Oceanic anoxia and the End Permian mass extinction. *Science* 272, 1155–1158.
- Wignall, P.B., Bond, D.P.G., Kuwahara, K., Kakuwa, Y., Newton, R.J., Poulton, S.W., 2010. An 80 million year oceanic redox history from Permian to Jurassic pelagic sediments of the Mino-Tamba terrane, SW Japan, and the origin of four mass extinctions. *Global and Planetary Change* 71, 109–123.
- Xie, S.C., Pancost, R.D., Huang, J.H., Wignall, P.B., Yu, J.X., Tang, X.Y., Chen, L., Huang, X.Y., Lai, X.L., 2007. Changes in the global carbon cycle occurred as two episodes during the Permian–Triassic crisis. *Geology* 35, 1083–1086.
- Xie, S.C., Pancost, R.D., Wang, Y.B., Yang, H., Wignall, P.B., Luo, G.M., Jia, C.L., Chen, L., 2010. Cyanobacterial blooms tied to volcanism during the 5 m.y. Permo-Triassic biotic crisis. *Geology* 38, 447–450.
- Xu, D.Y., Yan, Z., 1993. Carbon isotope and iridium event markers near the Permian/Triassic boundary in the Meishan Section, Zhejiang Province, China. *Palaeogeography, Palaeoclimatology, Palaeoecology* 104, 171–175.
- Yang, S., Hao, W., Wang, X., 1999. Conodont evolutionary lineages, zonation, and P–T boundary beds in Guangxi, China. In: Yao, A., Ezaki, Y., Hao, W., Wang, X. (Eds.), *Biotic and Geological Developments in the Paleo-Tethys in China*. Peking University Press, Beijing, pp. 81–95.
- Yang, H., Zhang, S.X., Jiang, H.S., Wang, Y.B., 2006. Age and general characteristics of the Calmicrobialite near the Permian–Triassic boundary in Chongyang, Hubei Province. *Journal of the China University of Geosciences* 17, 121–125.
- Yang, H., Chen, Z.Q., Wang, Y., Tong, J., Song, H., Chen, J., in press. Composition and structure of microbialite ecosystems following the end-Permian mass extinction in South China. *Palaeogeography, Palaeoclimatology, Palaeoecology*.
- Yin, H.F., Zhang, K., Tong, J.N., Yang, Z., Wu, S., 2001. The global stratotype section and point (GSSP) of the Permian–Triassic boundary. *Episodes* 24, 102–114.
- Yin, H.F., Feng, Q.L., Lai, X.L., Baud, A., Tong, J.N., 2007. The protracted Permo-Triassic crisis and the multi-episode mass extinction around the Permian–Triassic boundary. *Global and Planetary Changes* 55, 1–20.
- Zachos, J.C., Arthur, M.A., Dean, W.E., 1989. Geochemical evidence for suppression of pelagic marine productivity at the Cretaceous/Tertiary boundary. *Nature* 337, 61–64.
- Zeebe, R.E., Zachos, J.C., Dickens, G.R., 2009. Carbon dioxide forcing alone insufficient to explain Palaeocene–Eocene Thermal Maximum warming. *Nature Geoscience* 2, 576–580.
- Zhang, K.X., Tong, J.N., Yin, H.F., Wu, S.B., 1996. Sequence stratigraphy of the Permian–Triassic boundary section of Changxing, Zhejiang. *Acta Geologica Sinica* 70, 270–281 (in Chinese with English abstract).